HHS Public Access

Author manuscript

Sci Signal. Author manuscript; available in PMC 2021 April 20.

Published in final edited form as:

Sci Signal. ; 13(654): . doi:10.1126/scisignal.aaw3122.

Interclass GPCR heteromerization affects localization and trafficking

Rudy Toneatti[1], **Jong M. Shin**[1], **Urjita H. Shah**[1], **Carl R. Mayer**[2], **Justin M. Saunders**[1], **Miguel Fribourg**[4,5], **Paul T. Arsenovic**[2], **William G. Janssen**[3], **Stuart C. Sealfon**[4], **Juan F. López-Giménez**[1,6], **Deanna L. Benson**[3], **Daniel E. Conway**[2], **Javier González-Maeso**[1]

[1]Department of Physiology and Biophysics, Virginia Commonwealth University School of Medicine, Richmond, VA 23298, USA.

[2]Department of Biomedical Engineering, Virginia Commonwealth University College of Engineering, Richmond, VA 23220, USA.

[3]Department Neuroscience, Icahn School of Medicine at Mount Sinai, New York, NY 10029, USA.

[4]Department of Neurology, Icahn School of Medicine at Mount Sinai, New York, NY 10029, USA.

[5]Translational Transplant Research Center, Department of Medicine, Icahn School of Medicine at Mount Sinai, New York, NY 10029, USA.

[6]Instituto de Parasitología y Biomedicina “López-Neyra”, CSIC, E-18016 Granada, Spain.

Abstract

Membrane trafficking processes regulate G protein-coupled receptor (GPCR) activity. Although class A GPCRs are capable of activating G proteins in a monomeric form, they can also potentially assemble into functional GPCR heteromers. Here, we showed that the class A serotonin 5-HT_{2A} receptors (5-HT_{2A}R) affected the localization and trafficking of class C metabotropic glutamate receptor 2 (mGluR2) through a mechanism that required their assembly as heteromers in mammalian cells. In the absence of agonists, 5-HT_{2A}R was primarily localized within intracellular compartments, and coexpression of 5-HT_{2A}R with mGluR2 increased the intracellular distribution of the otherwise plasma membrane-localized mGluR2. Agonists for either 5-HT_{2A}R or mGluR2 differentially affected trafficking through Rab5-positive endosomes in cells expressing each component of the 5-HT_{2A}R-mGluR2 heterocomplex alone, or together. Additionally, overnight pharmacological 5-HT_{2A}R blockade with clozapine, but not with M100907, decreased mGluR2 density through a mechanism that involved heteromerization between 5-HT_{2A}R and mGluR2. Using TAT-tagged peptides and chimeric constructs that are unable to form the interclass 5-HT_{2A}R-mGluR2 complex, we demonstrated that heteromerization was necessary for the 5-

Corresponding author: javier.maeso@vcuhealth.org.

Author contributions: R.T. and J.G.M. designed experiments, analyzed data and wrote the manuscript. R.T. performed experiments. J.G.M. supervised research and obtained funding. J.M.S., U.H.S. and J.M.S. assisted with experiments. C.R.M. and P.T.A., supervised by D.E.C, performed the sensorFRET data analysis. M.F., supervised by S.C.S., performed ImageStream flow cytometry assays. W.G.J., supervised by D.L.B., performed electron microscopy assays. J.F.L.G. helped with assays in Flp-In T-REx HEK293 cells. All authors discussed the results and commented on the manuscript.

Competing interests: The authors declare that they have no competing interests.

Data and materials availability: All data needed to evaluate the conclusions in the paper are present in the paper or the Supplementary Materials.

HT_{2A}R-dependent effects on mGluR2 subcellular distribution. Expression of 5-HT_{2A}R also augmented intracellular localization of mGluR2 in mouse frontal cortex pyramidal neurons. Together, our data suggest that GPCR heteromerization may itself represent a mechanism of receptor trafficking and sorting.

INTRODUCTION

G protein-coupled receptors (GPCRs) are key membrane proteins involved in transduction of external signal across the cellular membrane into the cytoplasm of target cells (1-3). Although the majority of plasma membrane receptor proteins – including ion channels, transporters and enzyme-linked receptors – mature, behave and function as dimeric or oligomeric complexes, GPCRs have been assumed to be physiologically active as single monomeric units that interact with heterotrimeric G proteins upon agonist binding. However, GPCRs can also assemble as dimeric and oligomeric protein complexes (4-6) – a classic example is the essential role for heterodimerization in the trafficking and functional properties of the class C $GABA_B$ receptor (7). Thus, heterodimerization of $GABA_B$-R1 and $GABA_B$-R2 subunits is a prerequisite for the formation of a functionally active $GABA_B$ receptor as well as trafficking of $GABA_B$-R1 from the endoplasmic reticulum to the plasma membrane. Similar findings have been reported for other class C GPCRs, such as the metabotropic glutamate (mGlu) receptors, in which signaling induced by orthosteric agonist binding to the large extracellular domain necessitates a homodimeric receptor architecture (8, 9). Nevertheless, the concept of homodimerization/homomerization as a fundamental feature related to class A (also known as rhodopsin-like) GPCR activity, trafficking and localization remains a topic of debate.

Since the biochemical demonstration showing that a peptide derived from a β_2 adrenergic receptor transmembrane (TM) domain prevents both receptor complex formation and agonist-promoted stimulation of adenylyl cyclase activity (10), many groups have reported that class A GPCRs share the capacity to exist as dimers or higher oligomers [reviewed in (11, 12)]. Despite certain limitations and caveats of such biophysical approaches, including bioluminescence resonance energy transfer (BRET), Förster resonance energy transfer (FRET) and SNAP- or CLIP-tag (13, 14), these studies generally support the conclusion that class A GPCR homomerization is fundamental in controlling both agonist-induced receptor-G protein coupling (15, 16) and GPCR trafficking (17-21). Similarly, single molecule imaging studies in intact cells indicate that certain class A GPCRs form stable homomers (17, 22-24). Using similar experimental approaches, however, many others have shown either transient interactions (25-27) or absence of class A GPCR dimerization (28-30). Accordingly, many questions still remain open about the role of receptor complex formation in the dynamics and behavior of GPCRs.

Receptor trafficking, which involves maturation and insertion of newly synthesized receptors to the cell membrane (31), as well as processes related to internalization of GPCRs from the plasmalemma followed by subsequent recycling or degradation (32-35), is critical in controlling the net density of GPCRs at the cell surface. Hence, receptor trafficking processes dictate the number of receptor molecules that are available for interaction with

other signaling proteins and ligands. Ras-related GTPases of the Rab family regulate intracellular transport processes, including fusion of vesicles and organelle motility (33, 36). A subset of Rab proteins also controls certain types of endocytic and lysosomal pathways. Thus, early endosomes are regulated by Rab5, whereas lysosomal sorting involves the transfer of cargo proteins to late endosomes, which are marked Rab7.

With regards to class A GPCR complexes, effective homomerization of the α_{1B}-adrenoceptor has been suggested to be required for receptor maturation and surface delivery (19, 37). Similarly, agonist occupancy of a single protomer has been reported to be sufficient to cause internalization of the dimeric β_2-adrenergic receptor (18). Conversely, expression of serotonin 5-HT_{2A} receptors (5-HT_{2A}Rs) affects the agonist-induced subcellular distribution of μ-opioid (38) and CRF_1 (39) receptors in HEK293 cells. However, the extent to which GPCR heteromerization influences GPCR sorting processes in the endocytic pathway has been left unaddressed. In the present work, our interest was focused on the yet underexplored role of heteromerization in GPCR trafficking, using Rab5 and Rab7 as markers of early and late endosomes, respectively.

Class A serotonin 5-HT_{2A}R and class C metabotropic glutamate receptor 2 receptor (mGluR2) are GPCRs primarily coupled to $G_{q/11}$ and $G_{i/o}$ proteins, respectively. These two receptors participate in brain processes such as perception, cognition and sensorimotor gating, and have been implicated in psychiatric conditions such as schizophrenia, depression and alcoholism [reviewed in (40-42)]. Our previous findings (43-47), along with other studies (48-51), suggest that 5-HT_{2A}R and mGluR2 can form heteromeric complexes in living mammalian cells and ex vivo in rodent models. This molecular proximity, however, has not been observed in cells coexpressing 5-HT_{2A}R and mGluR3 (43-47). For the most part, GPCRs are primarily localized at the plasma membrane, particularly in cells not exposed to an agonist. However, certain GPCRs, including 5-HT_{2A}R, dopamine D_1 (52), δ-opioid (53) and GPRC6A (54) receptors, have a substantial intracellular presence. Thus, visualization of individual living cells shows that, at steady state, the bulk of 5-HT_{2A}Rs is present in punctate, intracellular vesicles (38, 39, 47, 55). Using electron microscopy approaches, the 5-HT_{2A}R also shows this intracellular localization in brain regions such as the frontal cortex and the ventral tegmental area (45, 56-59). During the course of our previous studies, we empirically showed that the mGluR2 alone is efficiently expressed on the cell surface, and that this archetypal localization of mGluR2 was affected by the presence of 5-HT_{2A}R (43, 45, 47). In the present study, we aimed to elucidate whether heteromerization underlies the mechanism responsible for the effect of 5-HT_{2A}R expression on mGluR2's subcellular redistribution.

RESULTS

5-HT_{2A}R affects subcellular distribution of mGluR2

To validate previous findings showing an elevated intracellular localization of the 5-HT_{2A}R, we imaged HEK293 cells expressing 5-HT_{2A}R tagged at the C-terminus with mCitrine (5-HT_{2A}R-mCitrine). As shown before (47, 60), the mCitrine signal was localized mostly in intracellular vesicles (Fig. 1A). To test whether this intracellular localization was due to a direct effect of the C-terminally tagged mCitrine on receptor trafficking, we also imaged

cells expressing 5-HT_{2A}R tagged at the N-terminus with c-Myc. Similar to 5-HT_{2A}R-mCitrine, c-Myc-5-HT_{2A}R construct was primarily located intracellularly (Fig. 1B).

We next asked whether cotransfection of the 5-HT_{2A}R and mGluR2 constructs affected the pattern of expression of these two receptors. In contrast with the subcellular localization observed in HEK293 cells transfected with the mGluR2-mCitrine construct alone (Fig. 1C, coexpression of 5-HT_{2A}R-mCherry affected the subcellular distribution of mGluR2-mCitrine (Figs. 1, D and E), which led to a high level of colocalization of mGluR2-mCitrine and 5-HT_{2A}R-mCherry in intracellular vesicles (fig. S1A).

Intracellular localization of the 5-HT_{2A}R-mGluR2 complex

To evaluate whether a direct physical interaction between 5-HT_{2A}R and mGluR2 is observable in intracellular vesicles, we used bimolecular fluorescence complementation (BiFC) as a biophysical technique that allows visualization of protein complexes in transfected mammalian cells (61). BiFC signal was detected in cells cotransfected with 5-HT_{2A}R fused to either the N-terminal 172 amino acid fragment or the C-terminal 67 amino acid fragment of mCitrine (mCi-N172 and mCi-C67, respectively) (Fig. 1F), which further corroborates the capability of 5-HT_{2A}R to form a class A GPCR homomer (47, 62-64). Additionally, BiFC signal in cells coexpressing 5-HT_{2A}R-mCi-N172 and 5-HT_{2A}R-mCi-C67 was observed intracellularly (Fig. 1F), whereas BiFC signal in cells coexpressing mGluR2-mCi-N172 and mGluR2-mCi-C67 was mostly detected at the plasma membrane (Fig. 1F). This pattern of BiFC signal was redistributed in cells coexpressing 5-HT_{2A}R-mCi-N172 and mGluR2-mCi-C67 (Fig. 1F), which suggests that physical interaction between 5-HT_{2A}R and mGluR2 can be detected both at the cell surface as well as intracellularly. Internal controls to validate specificity of this BiFC signal included cotransfection of mCi-N172 and mCi-C67 (fig. S2A), as well as mCi-C67 and 5-HT_{2A}R-mCi-N172, or mCi-C67 and mGluR2-mCi-N172 (fig. S2B).

Effect of 5-HT_{2A}R on subcellular localization of mGluR2 requires GPCR heteromerization

The Flp-In T-REx system allows expression of the inserted construct into the cell genome through Flp-In recombinase-mediated DNA recombination at the Flp recombination target (FRT) site, which can be controlled by the incorporation of the small molecule doxycycline (DOX) to the cell culture medium (65). This stable cell line model has previously been used to study receptor pharmacology, trafficking and oligomerization (22, 38). Here we used Flp-In T-REx HEK293 cells to further explore the effect of 5-HT_{2A}R on subcellular localization of mGluR2.

By using mGluR3 as well as an mGluR2/mGluR3 chimeric construct that does not form a GPCR heteromer with 5-HT_{2A}R, we devised an experimental system to test whether heteromerization was required to affect subcellular localization of mGluR2. We selected the mGluR2/mGluR3 chimeric construct mGluR2ΔTM4 because, according to our previous findings, substitution of residues $A677^{4.40}$, $A681^{4.44}$ and $A685^{4.48}$ in mGluR2 for $S686^{4.40}$, $F690^{4.44}$ and $G694^{4.48}$ in mGluR3 decreases heteromeric assembly (45). The c-Myc-5-HT_{2A}R-eCFP construct was inserted into the appropriate locus of the Flp-In expression system, and pools of positive Flp-In T-REx HEK293 cells were selected. No visible

expression of the eCFP-tagged construct was observed in the absence of DOX (fig. S3A). However, presence of DOX resulted in expression of the integrated construct as monitored by fluorescence corresponding to eCFP (fig. S3B) and immunoblotting with anti-c-Myc antibody (fig. S3C). Induction of expression of c-Myc-5-HT_{2A}R-eCFP was concentration- and time-dependent, reaching maximal levels within 30 – 40 h upon DOX (1 μg/ml) administration (figs. S3, B and C). Additionally, as shown above in HEK293 cells transiently transfected with the 5-HT_{2A}R construct, visualization of living Flp-In T-REx HEK293 cells corroborated that the bulk of c-Myc-5-HT_{2A}R-eCFP was located intracellularly (fig. S3B).

To explore whether the effect of 5-HT_{2A}R on intracellular localization of mGluR2 required GPCR heteromerization, cells exhibiting DOX-inducible expression of 5-HT_{2A}R-eCFP were transfected with various eYFP-tagged mGluR constructs and individual clones with eYFP signal were selected. In the absence of DOX, mGluR2-eYFP was largely at the cell surface (Fig. 2A). However, DOX-induced expression of 5-HT_{2A}R-eCFP increased the intracellular localization of mGluR2-eYFP (Fig. 2A), an effect that was not observed in cells stably expressing either mGluR3-eYFP (Fig. 2B) or mGluR2ΔTM4-eYFP (Figs. 2C). Compared to mGluR2-eYFP, both mGluR3-eYFP and mGluR2ΔTM4-eYFP showed a higher degree of intracellular localization, yet both quantitative evaluation (Fig. 2D and fig. S4a) and representative line scans (Figs. 2, E to G) demonstrated significantly less subcellular proximity between 5-HT_{2A}R-eCFP and mGluR3-eYFP or mGluR2ΔTM4-eYFP, as compared to the high degree of overlap between 5-HT_{2A}R-eCFP and mGluR2-eYFP. Subcellular distribution of the $G_{i/o}$ protein-coupled μ-opioid receptor, which is a plasma membrane-localized GPCR (38), was not affected by DOX-induced expression of 5-HT_{2A}R-eCFP (Figs. 2, H and I).

Radioligand binding assays with the 5-HT_{2A}R antagonist [^{3}H]ketanserin confirmed that the addition of DOX resulted in 5-HT_{2A}R-eCFP expression in cells stably expressing mGluR2-eYFP, mGluR3-eYFP or mGluR2ΔTM4-eYFP (figs. S5, A to C, and Table S1). Using the mGluR2/3 antagonist [^{3}H]LY341495, we also demonstrated that DOX-induced expression of 5-HT_{2A}R-eCFP led to a statistically significant increase in mGluR2-eYFP density, an effect that was not observed in cells stably expressing mGluR3-eYFP or mGluR2ΔTM4-eYFP (figs. S5, D to F, and Table S1). This effect of DOX-induced 5-HT_{2A}R-eCFP expression on augmentation of mGluR2-eYFP density was corroborated by fluorescence flow cytometry assays (figs. S5, G and H).

We next assayed the effect of the mGluR2/3 agonist LY379268 on stimulation of [^{35}S]GTPγS binding as a functional readout of receptor-$G_{i/o}$ protein coupling. DOX-induced expression of 5-HT_{2A}R-eCFP reduced the ability of LY379268 to increase [^{35}S]GTPγS binding in cells stably expressing mGluR2-eYFP (Fig. 2J), an allosteric event that was absent in cells stably expressing mGluR2ΔTM4-eYFP (Fig. 2K). As anticipated, LY379268 augmented G protein-dependent signaling in DOX(−) cells stably expressing mGluR2-eYFP, mGluR3-eYFP or mGluR2ΔTM4-eYFP (fig. S6A). These findings suggest that, although DOX-induced expression of 5-HT_{2A}R results in augmentation of total mGluR2 density, its functional properties for agonist-induced $G_{i/o}$ protein recruitment are diminished.

Our previous results showed that stimulation of cells coexpressing mGluR2 and 5-HT_{2A}R with the mGluR2/3 agonist LY379268 leads to a $G_{q/11}$ protein-dependent increase in the intracellular Ca^{2+} concentration ($[Ca^{2+}]_i$) (44, 46, 47), a trans-activation mechanism event that has been validated by some (66, 67) but not all (49) studies. LY379268 augmented $[Ca^{2+}]_i$ in DOX(+) cells stably expressing mGluR2-eYFP, an effect that was significantly reduced in DOX(+) cells stably expressing mGluR2ΔTM4-eYFP (Figs. 2, L and M). As expected, neither serotonin (5-hydroxytryptamine, 5-HT) nor LY379268 had such an effect on Ca^{2+} release in DOX(−) Flp-In T-REx HEK293 cells, whereas 5-HT stimulated an increase in intracellular Ca^{2+} release in DOX(+) cells (fig. S6B). This effect of 5-HT on Ca^{2+} release was absent untransfected HEK293 cells (fig. S6B).

To further explore the potential interaction between these two receptors, we tested protein association using two different methods. Using sensorFRET, which enables quantitative measurement of FRET efficiency (68), we observed a significant decrease in FRET efficiency between eCFP and eYFP in DOX(+) cells stably expressing mGluR2ΔTM4-eYFP as compared to that observed in cells stably expressing mGluR2-eYFP (Figs. 3, A to C and figs. S7, A to H). This finding confirms the impaired ability of the mGluR2/mGluR3 chimeric construct to physically interact with 5-HT_{2A}R. Moreover, the FRET signal between 5-HT_{2A}R-eCFP and mGluR2-eYFP was mostly located intracellularly in vesicles positive for both eCFP and eYFP fluorescence signal (Fig. 3A). Using proximity ligation assay (PLA) , which permits direct detection of molecular interactions between two proteins without needing resonance energy transfer assays (69), we found that following DOX-dependent induction of 5-HT_{2A}R-eCFP expression, the PLA signal between 5-HT_{2A}R and mGluR2 was observed in the form of punctate staining (Fig. 3D and fig. S8). Addition of DOX to cells harboring 5-HT_{2A}R-eCFP at the inducible locus and stably expressing mGluR2ΔTM4-eYFP resulted in significantly reduced PLA dot counts (Figs. 3, E and F). As anticipated, no PLA signal was detected in DOX(−) cells encoding 5-HT_{2A}R-eCFP at the inducible locus and stably expressing mGluR2-eYFP (Fig. 3F), or cells in which one of the primary antibodies was omitted (Fig. 3F).

Expression of 5-HT_{2A}R augments localization of mGluR2 in endosomal compartments

To evaluate the components of the intracellular trafficking pathway in which 5-HT_{2A}R affects subcellular distribution of mGluR2, we next tested the effect of DOX-induced expression of 5-HT_{2A}R on the colocalization of mGluR2 with endosomal markers. Confocal immunofluorescence microscopy in fixed cells revealed that colocalization of mGluR2-eYFP with Rab5, which regulates clathrin-mediated endocytosis from the plasma membrane to early/sorting endosome pools (33, 70), showed a modest, yet statistically significant, increase in DOX(+) cells as compared to DOX(−) cells (Figs. 4, A and B and figs. S1, B and C). Additionally, DOX-induced expression of 5-HT_{2A}R substantially augmented the localization of mGluR2-eYFP with the late endosome marker Rab7 (Figs. 4, C and D and figs. S1, E and F).

To quantitatively compare variant receptor trafficking and to validate our previous findings with an independent marker of clathrin-mediated endosomes, we assessed the colocalization of 5-HT_{2A}R-mCherry or mGluR2-eYFP with the transferrin receptor, which transits through

clathrin-coated pits and is a marker of early endosomes (33, 70) using imaging flow cytometry (46, 71). As above with Rab5 and Rab7, the localization between 5-HT_{2A}R-mCherry and the transferrin receptor was higher as compared to that observed between mGluR2-eYFP and transferrin receptor (fig. S9A). Additionally, whereas colocalization between 5-HT_{2A}R-mCherry and transferrin receptor was not affected upon cotransfection of the mGluR2-eYFP construct (fig. S9B), transfection of the 5-HT_{2A}R-mCherry construct led to a significant increase in the colocalization of mGluR2-eYFP and the transferrin receptor (fig. S9C).

DOI and LY379268 differentially affect mGluR2 localization in Rab5-positive endosomes

Our data thus far showed that, under steady state conditions, the colocalization of mGluR2 with markers of endocytic vesicles increased upon coexpression with 5-HT_{2A}R. However, agonist binding and activation of most GPCRs usually results in the rapid desensitization and endocytosis of the receptor. To gain further insight into how cells control subcellular localization of GPCR complexes, we next investigated the effects of different serotonergic and glutamatergic agonists on trafficking processes in cells coexpressing 5-HT_{2A}R and mGluR2.

To do so, we first explored the effect of the endogenous neurotransmitter 5-HT or the 5-HT_{2A}R agonist DOI on the localization of mGluR2 within Rab5-positive endosomes. Colocalization of mGluR2-eYFP and Rab5 was significantly increased after either 5-HT or DOI treatment in cells stably expressing mGluR2-eYFP and induced to express 5-HT_{2A}R-eCFP (Figs. 4, A and E, and figs. S1, C and D). As an internal control, we also confirmed that treatment with DOI did not affect the localization of mGluR2-eYFP and Rab5 in cells stably expressing mGluR2-eYFP and not induced (DOX[−]) to express 5-HT_{2A}R-eCFP (Fig. 4F). To test whether this trafficking event required heteromeric assembly between 5-HT_{2A}R and mGluR2, we used synthetic peptides with the amino acid sequence of TM4 of mGluR2 fused to the HIV transactivator of transcription (TAT) peptide, which determines the orientation of the peptide when inserted in the plasma membrane (72). First, as expected based on our previous findings (47, 73), incubation with TAT-TM4, but not with TAT-TM1 or a TAT-tagged scrambled peptide, significantly decreased the FRET signal in cells coexpressing 5-HT_{2A}R-eCFP and mGluR2-eYFP (Fig. 4G). Furthermore, incubation with TAT-TM4 reduced the effect of DOI on the colocalization of mGluR2-eYFP and Rab5 (Fig. 4H). Exposure to TAT-TM4, however, did not affect the colocalization between mGluR2-eYFP and Rab5 in vehicle-treated cells (Fig. 4H). The GTPase dynamin is essential for membrane fission during clathrin-mediated endocytosis (33). Dynasore inhibits dynamin-dependent endocytic pathways by rapidly blocking coated vesicle formation (74). The ability of DOI to increase the colocalization between mGluR2-eYFP and Rab5 was prevented by dynasore in DOX(+) cells (Fig. 4I). Flow cytometry assays with an Alexa Fluor 647 (AF647)-tagged antibody targeting the N-terminal of mGluR2 showed that cell surface localization of mGluR2-eYFP was increased by dynasore treatment, but unaffected by DOI in DOX(+) cells (Fig. 4J). This lack of effect of DOI exposure on cell surface mGluR2-eYFP was further supported by radioligand binding assays. Thus, [^{3}H]LY341495 binding was comparable in DOX(+) cells treated with DOI or vehicle (Fig. 4K). Together with the absence of effect of DOI treatment on FRET (Fig. 4L) and PLA (Fig. 4M) signal between 5-

HT_{2A}R-eCFP and mGluR2-eYFP, these data suggest that whereas exposure to DOI augments the localization of mGluR2 within Rab5-positive endosomes through a mechanism that requires heteromerization between 5-HT_{2A}R and mGluR2, activation of 5-HT_{2A}R does not affect mGluR2 cell surface density, total mGluR2 density, or mGluR2 heteromerization with 5-HT_{2A}R.

We next tested whether DOX-induced expression of 5-HT_{2A}R-eCFP modulates the effect of the mGluR2/3 agonist LY379268 on the subcellular localization and trafficking of mGluR2. As expected in DOX(−) cells, incubation with LY379268 led to both an increase in the colocalization between mGluR2-eYFP and Rab5 (Fig. 4N) and reduced cell surface AF647 signal (Fig. 4O), phenotypes that were prevented by dynasore (Figs. 4, O and P). This effect of LY379268 on the subcellular localization of mGluR2 was not observed in DOX(+) cells (Figs. 4, Q, R and S) but was rescued in DOX(+) cells by treatment with TAT-TM4 (Fig. 4T). Additionally, our radioligand bindings assays with the mGluR2/3 antagonist [^{3}H]LY341495 showed that mGluR2 density was reduced in DOX(−) cells treated with LY379268 (Fig. 4U), but not in cells stably expressing mGluR2-eYFP and induced to express 5-HT_{2A}R-eCFP (Fig. 4V). By contrast, in DOX-treated cells, the molecular proximity between 5-HT_{2A}R-eCFP and mGluR2-eYFP, as assessed by sensorFRET (Fig. 4L) and PLA (Fig. 4M), was reduced by previous exposure to LY379268. Together, these data show that the 5-HT_{2A}R agonist DOI and the mGluR2/3 agonist LY379268 differentially affect mGluR2 density as well as localization of mGluR2 with markers of endocytic compartments in cells expressing mGluR2 alone, or together with 5-HT_{2A}R.

Exposure to clozapine down-regulates mGluR2 through GPCR heteromerization with 5-HT_{2A}R

Previous reports suggested that the presence of 5-HT_{2A}R antagonists/inverse agonists affects intracellular localization of 5-HT_{2A}R constructs in living mammalian cell cultures. As an example, upon addition of ligands such as mianserin, cells show 5-HT_{2A}Rs predominantly at the plasma membrane (38). To corroborate these findings, we used Flp-In T-REx HEK293 cells expressing 5-HT_{2A}R-eCFP only (which means cells without stable expression of mGluR2-eYFP, mGluR3-eYFP or mGluR2ΔTM4) in an inducible manner. Following addition of DOX, cells were treated overnight with the 5-HT_{2A}R antagonist/inverse agonist M100907 (also known as volinanserin or MDL 100,907), or vehicle. In contrast to vehicle-treated cells, 5-HT_{2A}R-eCFP was essentially localized at the plasma membrane of cells treated with M100907 (Fig. 5A and figs. S1, G and H). Similar results were obtained with the 5-HT_{2A}R antagonist/inverse agonist altanserin (Fig. 5A and figs. S1, G and I). Together, these data suggest that, at steady state, the bulk of 5-HT_{2A}R-eCFP is present in punctate intracellular vesicles, and that treatment with the 5-HT_{2A}R antagonists/inverse agonists enhances the otherwise restricted cell surface localization of the 5-HT_{2A}R.

Clozapine is an antipsychotic medication that normally behaves as a 5-HT_{2A}R antagonist/inverse agonist, thus blocking or inhibiting 5-HT_{2A}R-dependent principal signaling pathways such as activation of $G_{q/11}$ proteins (75), yet can also activate certain pathways such as Akt (55). Additionally, and opposite to what is usually observed with most antagonists and inverse agonists, clozapine exposure did not discernibly affect the

subcellular distribution of 5-HT_{2A}R-eCFP in DOX(+) cells (Fig. 5A and figs. S1, G and J). Nevertheless, our previous findings in whole animal models showed that long-lasting exposure to clozapine induces mGluR2 down-regulation in brain regions such as the frontal cortex (43, 76, 77). Consequently, we tested whether clozapine affects mGluR2 localization and density in cells coexpressing 5-HT_{2A}R and mGluR2, as well as the requirement for 5-HT_{2A}R-mGluR2 heteromerization for this trafficking event.

Cells induced to express 5-HT_{2A}R-eCFP and stably expressing mGluR2-eYFP were incubated with clozapine or vehicle. As before (Fig. 2A), induction of 5-HT_{2A}R-eCFP corroborated a high degree of colocalization between 5-HT_{2A}R-eCFP and mGluR2-eYFP in intracellular vesicles of vehicle-treated cells (Fig. 5B and fig. S1K). Addition of clozapine resulted in an observable reduction of colocalization between mGluR2-eYFP and 5-HT_{2A}R-eCFP (Figs. 5, B and C, and figs. S1L and S4B). This effect was not observed after addition of M100907 (Figs. 5, B and D) and was prevented by TAT-TM4 (Fig. 5D). In contrast to cells expressing 5-HT_{2A}R-eCFP alone (Fig. 5A), both 5-HT_{2A}R-eCFP and mGluR2-eYFP remained intracellularly colocalized upon exposure to M100907 (Fig. 5B and fig. S1M). As expected (Fig. 2B), colocalization was less observable in cells coexpressing 5-HT_{2A}R-eCFP and mGluR2ΔTM4-eYFP (Figs. 5, C and E, and figs. S1N and S4B), yet this low degree of colocalization was not affected by clozapine (Figs. 5, C and E, and figs. S1O and S4B). Together, these data suggest that clozapine, and not M100907, reduces the subcellular colocalization of 5-HT_{2A}R-eCFP and mGluR2-eYFP through a mechanism that requires their molecular proximity.

We next tested whether clozapine treatment affected mGluR2 surface density through the 5-HT_{2A}R-mGluR2 heteromer. Our flow cytometry analysis showed that, in DOX(+) cells stably expressing mGluR2-eYFP, clozapine treatment reduced eYFP intensity (Fig. 5F), an effect that was not observed upon M100907 treatment (Fig. 5G) or in cells stably expressing mGluR3-eYFP (Fig. 5H). Similarly, density of mGluR2-eYFP, as determined by binding saturation curves with [^{3}H]LY341495, was reduced upon clozapine treatment in cells induced to express 5-HT_{2A}R-eCFP and stably expressing mGluR2-eYFP (Fig. 5I and fig. S10A). However, this clozapine-dependent effect was not observed in cells induced to express 5-HT_{2A}R-eCFP and stably expressing either mGluR3-eYFP (Fig. 5J and fig. S10B) or mGluR2ΔTM4-eYFP (Fig. 5K and fig. S10C). Treatment with clozapine also diminished both FRET efficiency (Fig. 5L) and PLA signal (Fig. 5M) between 5-HT_{2A}R-eCFP and mGluR2-eYFP. Although clozapine (Fig. 5N), but not M100907 (Fig. 5O), decreased the cell surface immunoreactivity of mGluR2-eYFP, this effect was more evident on the subpopulation of mGluR2 located intracellularly (Fig. 5P). Clozapine did not affect cell surface mGluR2-eYFP immunoreactivity (Fig. 5Q) or eYFP signal (Fig. 5R) in DOX(−) cells.

The absence of 5-HT_{2A}R affects the localization of mGluR2 in cortical pyramidal neurons

Neuroanatomical studies showed that 5-HT_{2A}R and mGluR2 colocalize in frontal cortex pyramidal neurons (43-45, 47). Our current data so far suggested that 5-HT_{2A}R modulated mGluR2 trafficking and localization in cultured mammalian cells. To ensure that this phenomenon occurred in a primary cell culture system, we examined whether localization of

mGluR2 in Rab5-positive endosomes was affected in cortical neuron cultures of 5-HT_{2A}R knockout (*5-$HT_{2A}R^{-/-}$*) mice and wild-type (*5-$HT_{2A}R^{+/+}$*) littermates. The colocalization of mGluR2 immunoreactivity and Rab5 was significantly reduced in cortical primary neuron cultures of *5-$HT_{2A}R^{-/-}$* mice as compared to *5-$HT_{2A}R^{+/+}$* animals (Figs. 6, A and B).

To assess whether the subcellular localization of mGluR2 could be regulated by its interactions with 5-HT_{2A}R in native tissue, we used immunogold labeling to examine mGluR2 distribution relative to the plasmalemma in the frontal cortex of *5-$HT_{2A}R^{+/+}$* and *5-$HT_{2A}R^{-/-}$* mice. We focused our analysis solely on excitatory postsynaptic dendritic spines which, in the frontal cortex region, are the principal sites of glutamatergic input onto pyramidal neurons (78-80). Our previous data showed that 5-HT_{2A}R and mGluR2 crosstalk in this population of cortical cells (43-45, 47). For each synapse, the distribution of particle clusters was scored based on their presence at the plasma membrane (fig. S11A), inside the cytoplasm (fig. S11B), or distributed on both plasmalemma and intracellularly (fig. S11C) In neurons from *5-$HT_{2A}R^{+/+}$* mice, the largest proportion of synapses showed both plasma membrane and intracellular labeling (Figs. 6, C and D). Additionally, there was a significantly greater proportion of gold particle clusters at the plasma membrane alone in neurons from *5-$HT_{2A}R^{-/-}$* mice relative to *5-$HT_{2A}R^{+/+}$* littermates (Figs. 6, C and D). Together, these findings indicate that subcellular localization of mGluR2 is affected by expression of 5-HT_{2A}R in mouse cortical pyramidal neurons.

DISCUSSION

The presence of multiple GPCRs in individual cells affects processes related to agonist-promoted GPCR endocytosis and down-regulation (19, 37, 81). For many GPCR heterocomplexes, such as δ-opioid-β_2-adrenergic (82), α_{2A} adrenergic-β_1-adrenergic (83), and adenosine A_{2A}-dopamine D_2 receptor (84) complexes, stimulation of only one of the components has been suggested to be sufficient to promote cotrafficking of the two protomers. Although interesting, it was assumed, but never clearly demonstrated, that heteromerization is the mechanism by which receptor coexpression evokes receptor cointernalization. In the present study, our data suggest that 5-HT_{2A}R affects the subcellular distribution of mGluR2 through a mechanism that requires a physical interaction of the two protomers. We show, further, that mGluR2 responds differently to processes related to agonist-induced targeting to endosomal compartments when expressed with 5-HT_{2A}R.

In addition, expression of 5-HT_{2A}R affects the subcellular distribution of mGluR2 in pyramidal neurons of the mouse frontal cortex.

Under steady state experimental conditions (absence of receptor agonists including the endogenous neurotransmitter 5-HT due to the use of dialyzed FBS in the culture media) our data validate the elevated level of localization of 5-HT_{2A}R in intracellular vesicles – a phenotype previously observed in HEK293 and CHO-K1 cells (38, 39, 55). Although an important proportion of the 5-HT_{2A}R population is located intracellularly, we and others have validated the expected finding that the addition of 5-HT_{2A}R agonists, including 5-HT or DOI, leads to activation of $G_{q/11}$ protein-dependent pathways, such as stimulation of the activity of phospholipase C (PLC) which increases intracellular inositol triphosphate (IP3),

diacylglycerol (DAG) and intracellular Ca^{2+} levels (46, 47, 85). Nevertheless, the effects of 5-HT_{2A}R antagonists or inverse agonists, such as M100907 and altanserin, on 5-HT_{2A}R subcellular localization and distribution of the receptor at the cell surface support the concept that 5-HT_{2A}R exhibits a high level of constitutive activity accounting for the intracellular localization of 5-HT_{2A}R. We showed that this distribution of 5-HT_{2A}R also affected the intracellular localization of mGluR2. The potential role of heteromerization as the mechanism underlying the effect of 5-HT_{2A}R on subcellular localization of mGluR2 was supported by our findings demonstrating intracellular BiFC, PLA and FRET signal coming from coexpression of appropriately tagged 5-HT_{2A}R and mGluR2 constructs. Recent findings point towards instability of a class A GPCR oligomeric interface (25, 27, 86). Our current data showing effects on trafficking and subcellular distribution through interclass GPCR heteromeric assembly support the concept that 5-HT_{2A}R and mGluR2 are part of a stable receptor complex structure. Further work, however, will be necessary to fully characterize the dynamics of this structural assembly.

An interesting observation was that whereas DOX-induced expression of 5-HT_{2A}R augments the density of mGluR2, but not that of mGluR3 or mGluR2ΔTM4, $G_{i/o}$ protein coupling induced upon activation of mGluR2 was substantially reduced in DOX(+) cells as compared to DOX(−) cells. Although this finding further supports specificity of the crosstalk between 5-HT_{2A}R and mGluR2, the exact mechanism remains to be investigated. Nevertheless, a potential explanation to reconcile these results is the existence of a compensatory pathway to rescue mGluR2-dependent function due to the higher degree of mGluR2 intracellular localization upon DOX-induced 5-HT_{2A}R expression.

Most GPCRs are transported to an endocytic pathway after internalization (33, 70). We showed that, in the absence of 5-HT_{2A}R or mGluR2 agonists, 5-HT_{2A}R colocalized with endosome marker proteins to a greater than mGluR2 in HEK293 cells expressing either protein alone. Our data also suggest that the presence 5-HT_{2A}R in cells stably expressing mGluR2 increased mGluR2 colocalization with different markers of the endocytic pathway such as Rab5, Rab7 and the transferrin receptor. Considering that colocalization of mGluR2 and Rab5 was also reduced in mouse cortical primary cultures of *5-$HT_{2A}R^{-/-}$* mice, these data suggest that 5-HT_{2A}R's constitutive internalization affects localization of mGluR2 within individual components of the endocytic pathway.

Acting through 5-HT_{2A}R, LY379268 and DOI differently affected the distribution of mGluR2 within Rab5-positive endocytic vesicles, as well as the physical interaction between 5-HT_{2A}R and mGluR2. Thus we found that whereas coexpression of 5-HT_{2A}R prevented the effect of mGluR2 agonists on both mGluR2 endocytosis and down-regulation, agonist-induced activation of mGluR2 decreased its physical proximity with 5-HT_{2A}R. Our data also support the conclusion that agonist activation of 5-HT_{2A}R increased the colocalization between mGluR2 and Rab5. This effect required 5-HT_{2A}R-mGluR2 heteromeric assembly because it was reduced by the peptide TAT-TM4. However, under the same experimental conditions, and opposite to the effects of LY379268, both mGluR2 density and 5-HT_{2A}R-mGluR2 heteromerization remained unchanged. These data suggest that whereas DOI augments intracellular distribution of mGluR2 within Rab5-positive and clathrin-dependent endosomes coexpressing 5-HT_{2A}R and mGluR2, internalized mGluR2 is not degraded after

entering the late-endosomal/lysosomal pathway. Sorting of mGluR2 into the recycling pathway could provide a potential explanation. Additional work will be necessary to determine the population of intracellular vesicles downstream of Rab5-positive endosomes responsible for increased endocytic uptake of mGluR2 without receptor downregulation.

In the absence of DOI, colocalization of mGluR2 and Rab5 was comparable between cells exposed to either TAT-TM4 or the TAT-tagged scrambled peptide. This absence of effect of TAT-TM4 on colocalization of mGluR2 and Rab5 at steady state conditions does not call into question the capability of the TAT-tagged peptide to reduce 5-HT_{2A}R-mGluR2 complex assembly. Instead, together with the effect of TAT-TM4 preventing DOI-induced augmentation of mGluR2 localization within Rab5-positive endosomes, these findings suggest that, in the absence of exogenous agonists such as DOI, disruption of 5-HT_{2A}R-mGluR2 heteromerization does not imply rapid mGluR2 trafficking from Rab5-positive endosomes to alternative endocytic compartments.

Although discovered in the late 1950s (87), clozapine still remains as the gold standard for schizophrenia treatment (75). It binds with relatively low affinity to dopamine D_2 and other monoaminergic neurotransmitter receptors, but similarly to other atypical antipsychotics, clozapine shows a particularly high affinity for 5-HT_{2A}R (88, 89). Activation of mGluR2 by mGluR2/3 agonists, including pomaglumetad or LY2140023 (an oral prodrug of LY404039), have been proposed to treat psychosis in schizophrenia patients (90), but pomaglumetad is not clinically useful (91). We previously proposed that chronic treatment with clozapine and other atypical antipsychotics induces a selective down-regulation of *mGluR2* expression through an epigenetic mechanism involving repressive histone modifications at the promoter region of the *mGluR2* (*Grm2*) gene in mouse and human frontal cortex (76, 77). These preclinical findings were validated by clinical work showing the absence of therapeutic effects of pomaglumetad in schizophrenia patients previously treated with atypical antipsychotic medications (92). Our current findings here propose an alternative, although not mutually exclusive, explanation by which long-lasting exposure to clozapine down-regulates mGluR2 density through a mechanism that requires its heteromerization with the 5-HT_{2A}R. We observed that subcellular colocalization between 5-HT_{2A}R and mGluR2 was reduced upon clozapine exposure. This effect was not induced by overnight exposure to M100907, was not observed in cells stably expressing mGluR2ΔTM4 and induced to express 5-HT_{2A}R, and was prevented by a TAT-tagged peptide that disrupts 5-HT_{2A}R-mGluR2 heteromerization. Similarly, clozapine, but not M100907, reduced total mGluR2 density as well as mGluR2 localization at both cell surface and in intracellular compartments. Thus, continued exposure to clozapine, but not M100907, affects mGluR2's subcellular distribution and density through a mechanism that requires 5-HT_{2A}R-mGluR2 complex formation. Further work will be necessary to better understand the trafficking pathway responsible for alterations in mGluR2 cellular distribution among 5-HT_{2A}R-positive intracellular vesicles and plasma membrane.

While some reported examples may reflect data overinterpretation or ambiguity due to the system in use, the concept that class A GPCRs form receptor complexes is supported by numerous experimental approaches. As of yet, the functional importance of GPCR oligomerization remains controversial. Our data obtained with stable expression of mGluR2

or mGluR2/mGluR3 chimeric constructs and TAT-tagged peptides to disrupt 5-HT_{2A}R-mGluR2 complex formation support the conclusion that 5-HT_{2A}R affects the subcellular localization of mGluR2 through GPCR heteromerization. The validity of this concept is further advanced by our findings showing alterations in mGluR2 cellular distribution in frontal cortex pyramidal neurons of *5-$HT_{2A}R^{-/-}$* mice as compared to control littermates. In short, these findings illuminate the importance of inter-family heteromerization on GPCR localization and trafficking.

Materials and Methods

Drugs

(±)-2,5-Dimethoxy-4-iodoamphetamine hydrochloride (DOI), 5-hydroxytrytamine hydrochloride (5-HT; serotonin), GDP, and GTPγS were purchased from Sigma-Aldrich. (1R,4R,5S,6R)-4-Amino-2-oxabicyclo[3.1.0]hexane-4,6-dicarboxylic acid (LY379268), (2S)-2-amino-2-[(1S,2S)-2-carboxycycloprop-1-yl]-3-(xanth-9-yl) propanoic acid (LY341495), clozapine, (*R*)-(+)-α-(2,3-dimethoxyphenyl)-1-[2-(4-fluorophenyl)ethyl]-4-piperinemethanol (M100907; MDL 100,907; volinanserin), 3-[2-[4-(4-fluorobenzoyl)-1-piperidinyl]ethyl]-2,3-dihydro-2-thioxo-4(1H)-quinazolinone hydrochloride (altanserin), L-glutamic acid, 3-hydroxynaphthalene-2-carboxylic acid (3,4-dihydroxybenzylidene)hydrazide (dynasore), and [8β(*S*)]-9,10-didehydro-*N*-[1-(hydroxymethyl)propyl]-1,6-dimethylergoline-8-carboxamide maleate (methysergide) were purchased from Tocris Bioscience. [^{3}H]Ketanserin and [^{35}S]GTPγS were obtained from PerkinElmer Life and Analytical Sciences. [^{3}H]LY341495 was purchased from American Radiolabeled Chemicals. All other chemicals were obtained from standard vendors.

Plasmid Construction

All PCR assays were performed with PfuUltra Hotstart Polymerase (Stratagene) in a Mastercycler Ep Gradient Auto thermal cycler (Eppendorf). Cycling conditions were 30 cycles of 94°C for 30 s, 55°C for 30 s, and 72°C for 1 min/kb of amplicon, with an initial denaturation/activation step at 94°C for 2 min and a final extension step of 72°C for 7 min. All the constructs were confirmed by DNA sequencing. The following constructs have been previously described (43, 45, 47): human 5-HT_{2A}R N-terminally tagged with the c-Myc epitope (pcDNA3.1-c-Myc-5-HT_{2A}R), human 5-HT_{2A}R N-terminally tagged with the c-Myc epitope and C-terminally tagged with enhanced cyan fluorescent protein (pcDNA3.1-c-Myc-5-HT_{2A}R-eCFP), human 5-HT_{2A}R N-terminally tagged with the c-Myc epitope and C-terminally tagged with mCitrine (pcDNA3.1-c-Myc-5-HT_{2A}R-mCitrine), human 5-HT_{2A}R N-terminally tagged with the c-Myc epitope and C-terminally tagged with mCherry (pcDNA3.1-c-Myc-5-HT_{2A}R-mCherry), human 5-HT_{2A}R N-terminally tagged with the c-Myc epitope and C-terminally tagged with eYFP (pcDNA3.1-c-Myc 5-HT_{2A}R-eYFP), human mGluR2 C-terminally tagged with eYFP (pcDNA3.1-mGluR2-eYFP), human mGluR2 C-terminally tagged with eCFP (pcDNA3.1-mGluR2-eCFP), human mGluR3 C-terminally tagged with eYFP (pcDNA3.1-mGluR3-eYFP), human mGluR2 with substitution of residues A677$^{4.40}$, A681$^{4.44}$ and A685$^{4.48}$ in mGluR2 for S686$^{4.40}$, F690$^{4.44}$ and G694$^{4.48}$ in mGluR3 C-terminally tagged with eYFP (pcDNA3.1-mGluR2ΔTM4; formerly named pcDNA3.1-mGluR2ΔTM4N). The construct 5-HT_{2A}R-eCFP was subcloned into the

vector pcDNA5/FRT/TO (Invitrogen) for the subsequent generation of Flp-In T-REx HEK293 cells, as we have previously reported (38). For BiFC studies, constructs were generated by subcloning the sequence encoding the N-terminal 172-amino acid fragment (mCi-N172) or the C-terminal 67 amino acid fragment of mCitrine (mCi-C76), as we have previously described [see (19)]. The constructs pcDNA3.1-mCi-N172, pcDNA3.1-mCi-C67, pcDNA3.1-mGluR2-mCi-N172 and pcDNA3.1-mGluR2-mCi-C67 have been previously described (47). The form of 5-HT_{2A}R C-terminally tagged with eCFP was digested with NheI and BamHI and subcloned into the same restriction sites of pcDNA3.1-mCi-N172 and pcDNA3.1-mCi-C67 to generate pcDNA3.1-5-HT_{2A}R-mCi-N172 and pcDNA3.1-5-HT_{2A}R-mCi-C67. The chimeric Gα protein $G\alpha_{qi9}$ has been previously reported (93). FRET calibration was performed on parental HEK293 cells transfected with either pcDNA3.1-eCFP, pcDNA3.1-eYFP, or the tandem plasmid pcDNA3.1-eCFP-eYFP.

Transient Transfection of HEK293 cells

Human embryonic kidney (HEK293) cells (ATCC: CRL-1573) were maintained in Dulbecco's modified Eagle's medium (DMEM) supplemented with 10% (v/v) dialyzed fetal bovine serum (dFBS) and 1% penicillin/streptomycin (Gibco) in a 5% CO_2 humidified atmosphere. Transfection was performed using polyethylenimine (PEI) linear MW 2,500 (Polysciences), following standard protocols.

Generation of Stable Flp-In T-REx HEK293 cell lines

Generation Flp-In T-REx HEK293 cells expressing c-Myc-5-HT_{2A}R-eCFP in an inducible manner was preformed following standard protocols (65). Briefly, Flp-In T-REx HEK293 cells were transfected with a mixture containing either c-Myc-5-HT_{2A}R-eCFP cDNA in the pcDNA5/FRT/TO vector and pOG44 vector (1:9) using Lipofectamine 2000 reagent (Invitrogen), according to the manufacturer's instructions. When cotransfected with the pcDNA5/FRT/TO plasmid into the Flp-In mammalian host cell line, the Flp recombinase expressed from pOG44 mediates integration of the pcDNA5/FRT/TO vector containing the gene of interest into the genome through Flp recombination target (FRT) sites. Clones resistant to blasticidin (5.0 μg/ml; InvivoGen) and hygromycin (2.2 μg/ml; InvivoGen) and expressing the Tet repressor (tetR) along with the inserted c-Myc-5-HT_{2A}R-eCFP at the FRT site were screened for eCFP expression by standard fluorescence microscopy protocols.

Double stable cell lines expressing mGluR2-eYFP, mGluR3-eYFP or mGluR2ΔTM4 constitutively and 5-HT_{2A}R-eCFP in an inducible manner were generated from the Flp-In T-REx HEK293 cells described above. Cells were transfected using Lipofectamine 2000 reagent (Invitrogen) with the vectors containing mGluR2-eYFP, mGluR3-eYFP or mGluR2ΔTM4. Following transfection, cells were selected for resistance to Geneticin (1 mg/ml; Invitrogen), and the resistant clones were screened for receptor expression by standard fluorescence microscopy. Flp-In T-REx HEK293 cells stably expressing μ-opioid receptor tagged with eYFP and able to express c-Myc-5-HT_{2A}R-eCFP in an inducible manner have previously been described (38).

To induce expression of 5-HT_{2A}R-eCFP, cells were treated with doxycycline (DOX) (1.0 μg/ml; 24 – 48 h). Dialyzed FBS was used for cell growth to avoid activation of 5-HT_{2A}R by 5-HT that is routinely present in serum.

Mice

5-HT_{2A}R knockout (*Htr2a*$^{-/-}$) mice of 129S6/Sv background have previously been described (94). For experiments involving *5-HT*$_{2A}$*R*$^{-/-}$ mice, wild-type (*5-HT*$_{2A}$*R*$^{+/+}$) littermates on a 129S6/Sv background were used as controls. Animals were housed at 12 h light/dark cycle at 23°C with food and water ad libitum. The Institutional Animal Use and Care Committee at Virginia Commonwealth University School of Medicine approved all the experimental procedures.

Cortical primary cultures

Fetuses (E17-18.5) from pregnant mothers were removed using aseptic techniques. Cortical primary cultures were performed as previously reported (94). Cells were maintained for 7 days in vitro before use in experiments.

Immunocytochemistry

In HEK293 cells or mouse cortical primary cultures, immunocytochemical assays were performed as previously reported with minor modifications (43-45, 47). Briefly, cells were fixed with 4% paraformaldehyde (Sigma) supplemented with 100 μM $CaCl_2$ and 100 μM $MgCl_2$ for 10 min at room temperature, rinsed with PBS, and washed twice with PBS supplemented with 20 mM glycine. Coverslips were incubated with 0.2% Triton X-100 for 10 min at room temperature and incubated in the dark for 60 min with PBS containing 5% donkey or goat serum (according to the secondary antibody). Primary antibody was added (40 μl on each coverslip) and incubated overnight at 4°C. Primary antibodies used were rabbit anti-c-Myc (Cell Signaling Technology catalog no. 2272; diluted at 1:250), mouse anti-mGluR2 (Abcam catalog no. 15672; diluted at 6.5 μg/ml), goat anti-Rab5 (SICGEN catalog no. ab1024; diluted at 6.5 μg/ml [HEK293 cells] or 5.0 μg/ml [primary neurons]), rabbit anti-Rab7 (Cell Signaling Technology catalog no. 9367; diluted at 1:100), or rabbit anti-GFP (Invitrogen catalog no. A11122; diluted at 1:500) After washing with PBS, cells were incubated for 60 min at room temperature in the dark with the secondary antibodies Alexa Fluor 488-conjugated goat anti-rabbit (Invitrogen catalog no. A11011; dilution 1:1000), Alexa Fluor 568 conjugated goat anti-rabbit (Invitrogen catalog no. A11004; dilution 1:1000), Alexa Fluor 568-conjugated donkey anti-goat (Invitrogen catalog no. A11057; dilution 1:1000), or Dylight 650-conjugated donkey anti-mouse (Thermofisher catalog no. SA5-10169 [primary neurons]). Nuclei were stained (5 min) with Hoechst 33342 (ThermoScientific). After washing (PBS, 6 × 5 min), the coverslips were mounted on glass slides with Prolong Diamond Antifade Mountant (ThermoFisher).

Confocal microscopy

Fixed cells and living cells were visualized on a Carl Zeiss Axio Observer LSM 710 laser scanning confocal microscope (LSCM) with a Plan-Apochromat 63×/1.40 Oil DIC M27 or 40× Cal objective. Hoechst 33342 was excited by a 405 nm blue diode, and eCFP with a 440

nm laser-pulse. Additionally, 488 nm and 514 nm multi-line Argon lasers were used to excite Alexa Fluor 488, mCitrine and eYFP, respectively, whereas a 561 nm green diode laser was used to excite mCherry and Alexa Fluor 568. Finally, DyLight 650 was excited with a 633 nm HeNe laser line. Emission signals were acquired in the same order using the following Main Beam Splitter/Dichroic Beam Splitter (MBS/DBS) and emission filters (EF) sets: InVis 405/Mirror EF: 410-482nm, InVis 445/Mirror EF: 435-480 nm, 488/Mirror EF: 494-523 nm, 458/514/Mirror EF: 523-543 nm, and 458/561/633/Mirror EF: 591-661 (mCherry) 573-620 (AF568) 654-700 (DyLight650). Pinhole was kept constant and adjusted at 1 airy unit. Living cells (cell cloning) were visualized on a Carl Zeiss Cell Axio Observer Z1 spinning disc confocal microscope (SDCM) with an embedded Yokogawa CSU-X1 spinning disc and a C-Apochromat 63×/1.20 W Korr UV-Vis-IR objective. Illumination sources were a 458 nm and 514 nm (multi-Ar) laser for eCFP and eYFP, respectively. Emission filters (SD mirror + bypass filters BP) were RTFT457/514/647 + BP485/30 (eCFP) and RQFF405/488/568/647 + BP525/50 (eYFP). During image acquisition, cells were maintained at 37°C and 5% CO2 atmosphere by an incubation system.

Immunoblot Assays

Western blot experiments were performed as previously reported (45), using rabbit anti-c-Myc (Cell Signaling, catalog no. 2272; diluted at 1:400) and rabbit anti-β-actin (Abcam catalog no. 8227; diluted at 0.33 μg/ml).

TAT-fused transmembrane domain interference peptides

Peptides derived from human mGluR2 TM4 and TM1 were custom synthesized (Genemed Synthesis, Inc.). TAT (trans-activating transcriptional activator from human immunodeficiency virus; YGRKKRRQRRR) was fused to the N-terminus of the human mGluR2 TM4 (YGRKKRRQRRRSPASQVAICLALISGQLLIVVAWLVVE) and TM1 (AWAVGPVTIACLGALATLFVLGVFVRHYGRKKRRQRRR) to obtain the correct orientation for the inserted peptide because TAT binds to phosphatidylinosityol-(4,5)-biphosphate found on the inner surface of the membrane (72). TAT-labelled 38-mer peptide was used as an internal control (YGRKKRRQRRRVIAPLYTSCVNWQIFVISMYRGARVAI). Stock solutions of the TAT-tagged peptides (5.2 mM) were prepared in DMSO supplemented with glacial acetic acid (1.93%). For FRET assays, cells were incubated with TAT-tagged peptides (10 μM, final concentration) for 60 min (DMSO's final concentration = 0.18%). For studies involving receptor agonists, TAT-tagged peptides were added 5 minutes before DOI or LY379269, or vehicle administration. For studies involving overnight treatment with clozapine, TAT-tagged peptides were added both 5 minutes before clozapine or vehicle administration and 65 minutes before cell fixation.

Proximity Ligation Assay

Heteromers of c-Myc-5-HT_{2A}R-eCFP and mGluR2-eYFP were detected using the Duolink In Situ PLA Detection Reagents Red technology kit (Sigma-Aldrich). Briefly, coverslips with fixed cells were incubated with 0.1% Triton X-100 for 10 min at room temperature then in blocking solution according to manufacturer's instructions. Cells were incubated overnight at 4°C with a mixture of the primary antibodies (rabbit anti-c-Myc [Cell Signaling

Technology, catalog no. 2272; 1:250], and mouse anti-mGluR2 [Abcam, catalog no. 15672; 1:200]). Samples were incubated with Duolink In Situ PLA Probe Anti-Rabbit PLUS Affinity purified Donkey anti-Rabbit IgG and Duolink In Situ PLA Probe Anti-Mouse MINUS Affinity purified Donkey anti-Mouse IgG. Samples were processed for ligation and amplification and were mounted onto glass slides with Prolong Diamond Mountant. Z-stack images were acquired in a Carl Zeiss Axio Observer LSM 710 laser scanning confocal microscope with a Plan-Apochromat 63×/1.40 Oil DIC M27 objective (to obtain a representative image) or 40× Cal objective (for quantification purposes). For each field of view, a stack of three channels (one per staining) was obtained. Images were processed with Fiji software version 2.0.0 (National Institutes of Health, Bethesda, MD). To quantify PLA signal, PLA-red channel remained hidden during cell identification process. Automated counting involved selection and cropping of each region of interest, Z-Stack projection of the PLA channel, subtraction of background with a rolling ball radius of 20 pixels and finding maxima with a noise tolerance value of 6000–10000 depending on the experiment and the background.

Radioligand binding assays

[^{3}H]Ketanserin, [^{3}H]LY341495 and [^{35}S]GTPγS binding assays were performed as previously reported (43-45, 47). The stoichiometry of 5-HT_{2A}R density (as assessed by [^{3}H]ketanserin binding) and mGluR2 density (as assessed by [^{3}H]LY341495 binding) is similar to that previously observed in native tissue, such as mouse frontal cortex and postmortem human frontal cortex (43-45, 47) and in cross-talk positive clones (46).

$[Ca^{2+}]_i$ Mobilization assays

Two days before the assay, cells were plated onto poly-D-lysine coated 96-well plates (Greiner Bio-One GmbH) and, 48 hours later, treated with doxycycline (1 μM) for 40 h. Cells were washed with DPBS and loaded with 3 μM Fura 2-AM (Molecular Probes) in imaging solution (5 mM KCl, 0.4 mM KH_2PO_4, 138 mM NaCl, 0.3 mM Na_2HPO_4, 2 mM $CaCl_2$, 1 mM $MgCl_2$, 6 mM glucose, 20 mM HEPES, pH 7.4) supplemented with pluronic acid (20% solution in DMSO). After incubation for 30 min at 37°C, cells were washed twice with washing buffer before being placed on the FlexStation 3 microplate reader (Molecular Devices). The Fura-2 signal was acquired at 510 nm by switching the excitation wavelength between 340/380 nm. Intracellular calcium concentration was expressed as a 340/380 nm ratio, and values were normalized to the basal 340/380 nm ratio recorded during 30 seconds before perfusion of the drug using Softmax Pro (Molecular Devices). To allow efficient coupling of $G_{i/o}$-coupled mGluRs to the PLC pathway, cells were also transfected with the chimeric Gα protein $G\alpha_{qi9}$ (93). Concentrations of LY379268 were selected based on our previous findings (47). Thus, activation of the canonical $G_{i/o}$ protein-dependent pathway was tested in the presence of LY379268 (0.1 μM), but trans-activation of the $G_{q/11}$ protein-dependent pathway was tested in the presence of LY379268 (10 μM and 100 μM).

Flow cytometry and immunofluorescence

Cells were treated with for 60 min with either DOI (1 μM), LY379268 (10 μM), or vehicle, or (overnight) with clozapine (10 μM) M100907 (10 μM) or vehicle. Cells were trypsinized, washed with PBS, filtered through filter top tubes (35 μm), resuspended in PBS

supplemented with 1% FBS, and analyzed using a LSRFortessa X-20 Flow cytometer (BD Bioscience). eCFP and eYFP were excited with a 405 nm and a 488 nm laser line, respectively. Emission filters were 525/50 and YFP-A. Quantification was carried out using FCS Express v.5 (De Novo Software). Mean intensity values were determined by gating 25.5% or more of the total cell population. Imaging flow cytometry (Amnis ImageStreamX) to measure colocalization of mGluR2 or 5-HT_{2A}R with the transferrin receptor at the single cell level was performed as previously reported, using an Amnis ImageStream flow cytometer (46). Cells were considered to present a colocalized signal between the receptor constructs and transferrin receptor when their Bright Detail Similarity score was greater than 2. To detect cell surface receptors, cells were treated with DOI, LY379268 or vehicle (60-min treatment), or with clozapine, M100907 or vehicle (overnight treatment). Cells were washed with ice-cold imaging buffer (PBS supplemented with 10% FBS) and incubated with human mGluR2 Alexa Fluor 647-conjugated antibody (R&D Systems, catalog no. IC4676R; 1:40) for 60 min on ice (~11-13°C). After two washes with ice-cold imaging buffer, cells were resuspended in ice-cold imaging buffer and loaded into the flow cytometer. 405 nm, 488 nm and 640 nm lasers were used to excite eCFP, eYFP and AF647, respectively. Data were subsequently gated and analyzed using the FCS Express 5 software.

SensorFRET

SensorFRET assays were performed as previously reported (68). Briefly, the fluorophores associated with uneven expression levels between the donor and acceptor. The fluorophores used as the FRET pair were eCFP (donor) and eYFP (acceptor) with quantum yields assumed to be 0.40 and 0.61, respectively (95). This approach also requires knowledge of the fluorophore emission shapes (for linear unmixing of the spectra) as well as the relative molar extinction coefficients for the fluorophores at each excitation frequency (characterized by the γ parameter). The normalized emission shapes of both fluorophores as well as the autofluorescence at each excitation frequency were determined experimentally. The γ calibration term was also determined experimentally ($\gamma = 0.114$), following a previously described procedure (68). Imaging was carried out using a Zeiss 710 confocal LSM at 405nm and 458 nm excitation frequencies and a 32-channel spectral detector spanning an emission range of 416nm to 718nm. In unfixed cells, short acquisition times (~600 ms) were necessary to minimize the shift due to vesicle movement during the time needed to acquire images at both excitation wavelengths. For assays involving TAT-tagged peptides, cells were briefly fixed with PFA (1%) for 5 min to avoid background caused by PFA fixation. A minimum of 30 cells were imaged for each experimental group. For the statistical analysis, the measured FRET efficiency of each vesicle was considered a single observation. Strict masking was carried out to include vesicles that met three criteria. First, only vesicles which remained stationary between the 405 and 458 nm images were included because even at short acquisition times, some population of vesicles showed appreciable movement. Second, only vesicles with a donor to acceptor stoichiometry within the range of 1:10 to 1:1 were included because the sensorFRET approach is not applicable when there are excess donor fluorophores (68). Thus, below a 1:10 ratio the donor signal is so small that it is difficult to reliably distinguish it from auto fluorescence and noise. The stoichiometry was estimated by comparing the ratio of the donor and acceptor direct excitation in experimental vesicles to a unimolecular construct (both CFP and YFP are encoded as part of the same protein) where

the stoichiometry is known to be 1:1. Marks were drawn only over pixels that showed colocalized eCFP and eYFP signal from both 405 nm and 458 nm images. Finally, only vesicles consisting of greater than 5 pixels were included so that mis-localization of proteins to small non-vesicle features was excluded, allowing each vesicle observation to be the average of multiple spectra and improving the signal to noise ratio.

Electron Microscopy

Electron microscopy assays were carried out as previously reported with minor modifications (45). Briefly, four mice (8 – 12 weeks old) per genotype were deeply anesthetized and perfused transcardially with 2% dextran (MW 70,000) in 0.1 M phosphate buffer (PB, pH 7.4), and then with a mixture of 4% paraformaldehyde and 0.125% glutaraldehyde in phosphate buffered saline (PBS). Brains were removed and post-fixed in the same perfusate overnight at 4°C. Approximately 0.5-mm-thick coronal slices were dissected from the regions of interest. Tissue blocks through superficial layers of prefrontal cortex were embedded in Lowicryl HM20 resin (Electron Microscopy Sciences, Fort Washington, PA) by freeze substitution and low-temperature embedding of the specimens using methods previously described (96-98). Briefly, slices were cryoprotected by immersion in 4% D-glucose, followed with increasing concentrations of glycerol (from 10% to 30% PB). Sections were plunged rapidly into liquid propane cooled by liquid nitrogen (−190°C) in a Universal Cryofixation System KF80 (Reichert-Jung, Vienna, Austria). The samples were immersed in 0.5% uranyl acetate dissolved in anhydrous methanol (−90°C, 24 h) in a cryosubstitution AFS unit (Leica, Vienna, Austria). The temperature was raised from −90°C to −45°C in steps of 4°C/h. After washing with anhydrous methanol, the samples were infiltrated with Lowicryl HM20 resin at −45°C. Polymerization with ultraviolet light (360 nm) was performed for 48 h at −45°C, followed by 24 h at 0°C. Ultrathin sections (80 nm) were cut using a diamond knife on a Leica UC7 ultramicrotome, and mounted on 300 mesh nickel grids (EMS) coated using a Coat-Quick adhesive pen (EMS). Grids with sections were incubated in 0.1% sodium borohydride and 50 mM glycine for 6 minutes at room temperature, washed and incubated for 10 min in Tris-buffered saline with 0.1% Triton X-100 (TBST) containing 2% albumin. For immunolabeling, sections were incubated overnight in primary anti-mGluR2 antibody (Abcam, mouse monoclonal antibody catalog no. 15672, 10 μg/ml) in the same diluent as above, washed with TBST, and incubated with secondary anti-goat 10 nm gold-tagged antibody (EMS; 1:20) in TBST (2% albumin and polyethyleneglycol 20,000; 5 mg/ml) for two hours, washed and counter-stained with 1% uranyl acetate (aq.). The specificity of the primary antibody against mGluR2 was previously confirmed in experiments with knockout mice (45). Grids were viewed on a Hitachi 7000 transmission electron microscope and imaged at a final captured image magnification of 130K. Imaging concentrated on deep layer 2-3 of the prefrontal cortex. Excitatory (asymmetric) glutamatergic synapses were identified by the presence of a thickened postsynaptic density, synaptic cleft, and clusters of round presynaptic vesicles (99). A synapse was scored as immunolabel-positive if it contained at least 3 gold particles in the synaptic compartments described above, and 25-35 labeled synapses were imaged per animal/group. Overall, ~90% of labeled synapses showed gold particles associated within the postsynaptic element, though a small population of synapses contained gold particles limited to its presynaptic compartment. Gold particle distribution with respect to

plasmalemma was scored for each postsynaptic site as membrane only, intracellular only, or both. Membrane labelling was defined by gold particles falling within 25 n of the plasmalemma (a distance defined by the approximate size of the primary and secondary antibodies).

Data acquisition and statistical analysis

Statistical analysis was performed with a GraphPad Prism software version 8. Immunocytochemical assays were acquired using confocal fluorescence microscopy at identical settings for each of the experimental conditions. For colocalization assays, raw 16-bit image files (.czi) were imported into the Carl Zeiss ZEN software (Black version) and/or Fiji version 2.0.0 with Coloc 2 plugin. To assess colocalization, Pearson's and/or Manders' coefficients were calculated because these colocalization coefficients are based on pixel-intensity-correlation measurement and do not include object-recognition approaches. Pearson's coefficient, which ranges from +1 (total positive linear correlation) to −1 (total negative correlation; 0 defines absence of linear correlation) is sensitive to both signal cooccurrence and the more rigorous condition of signal correlation (pixel-for-pixel proportionality in the signal levels of the two channels). However, unlike Pearson's correlation coefficient, Manders' fractional overlap coefficients (M1 and M2), which measure the fraction of a probe in a probe-tagged compartment and range from 0 (no overlap) to 1 (perfect overlap), strictly measures cooccurrence independent of signal proportionality (100, 101). Colocalization of two fluorescently labelled GPCR constructs (5-HT_{2A}R-eCFP and mGluR2-eYFP) was assessed both by Manders' and Pearson's coefficients, whereas colocalization of a fluorescently labelled GPCR construct with a marker of endosomal vesicles (Rab5) was assessed by Manders' coefficient. Both Manders' and Pearson's coefficients within the region of interest were calculated after setting single color thresholds by either colocalizing single probe channels or manually defining a threshold mask upon background subtraction in all channels using Rolling Ball Radius of the largest object in the image (~ 20 – 30 μm). Colocalization was scored in at least 25 cells per experimental condition in three independent assays where the experimenter was blinded to the experimental conditions. For Manders' and Pearson's coefficients, cell regions of interest were demarcated according to the eYFP signal located at the plasma membrane as a potential cell surface marker. For FRET signal, pixels of interest were demarcated based on their intracellular colocalization of eCFP and eYFP signal. For PLA signal, cell regions of interest were demarcated according to eYFP signal within previously defined eCFP-positive cells. For intracellular eYFP signal, cell regions of interest were randomly demarcated based on eCFP signal within intracellular vesicles. Signal intensity for intracellular eYFP was assessed with the Carl Zeiss ZEN software (Black version). The laser intensity was kept constant among all experimental conditions. Straight-line selections were drawn from the plasma membrane to the nucleus or across the cytoplasm, and pixel intensities across the line were measured using plot profile in Fiji. Pixels with maximum and minimum intensities were normalized to 100 and 0, respectively. The statistical significance of experiments involving three or more groups and two or more treatments was assessed by two-way ANOVA followed by Bonferroni's post hoc test. Statistical analysis of experiments involving three or more groups was assessed by one-way ANOVA followed by Bonferroni's post hoc test. Statistical analysis involving two groups was assessed by Student's *t*-test. For

FRET analysis, statistical analysis was assessed by Mann-Whitney U test or one-way non-parametric ANOVA (Kruskal-Wallis) with Dunn's post hoc test because FRET datasets show a Cauchy distribution with heavier tails. Radioligand binding saturation curves were analyzed using a nonlinear curve fitting approach. An extra-sum-of-squares (F test) was used to determine statistical significance for simultaneous analysis of binding saturation curves and [^{35}S]GTPγS binding assays. The level of significance was set at $P = 0.05$. Values included in the figure legends represent mean ± SEM, except for FRET assays where figure legends represent median with 95% confidence interval.

Supplementary Material

Refer to Web version on PubMed Central for supplementary material.

Acknowledgements:

The authors thank Philippe Rondard (University of Montpellier) for the donation of the Gα_{qi9} construct, Sergi Ferré (NIDA) for his advice on experiments with TAT-linked peptides, and Tytus Bernas, Mikhail Dozmorov and Julie Farnsworth (Virginia Commonwealth University) for their help in microscopic imaging, biostatistical analysis and flow cytometry assays, respectively.

Funding: NIH R01 MH084894 (J.G.M.), NIH R01 MH111940 (J.G.M.), NIH R01 MH103455 (D.L.B), NIH R01 DK046943, (S.C.S), NIH R35GM119617 (D.E.C.), and NIH F30 MH116550 (J.M.S.) provided funding of this study. Microscopy Shared Resource and Flow Cytometry Core at VCU were supported, in part, with funding from NIH-NCI Cancer Center Support Grant P30 CA016059.

REFERENCES AND NOTES

1. Weis WI, Kobilka BK, The Molecular Basis of G Protein-Coupled Receptor Activation. Annu Rev Biochem 87, 897–919 (2018). [PubMed: 29925258]
2. Hilger D, Masureel M, Kobilka BK, Structure and dynamics of GPCR signaling complexes. Nat Struct Mol Biol 25, 4–12 (2018). [PubMed: 29323277]
3. Erlandson SC, McMahon C, Kruse AC, Structural Basis for G Protein-Coupled Receptor Signaling. Annu Rev Biophys (2018).
4. Ferre S, Casado V, Devi LA, Filizola M, Jockers R, Lohse MJ, Milligan G, Pin JP, Guitart X, G protein-coupled receptor oligomerization revisited: functional and pharmacological perspectives. Pharmacol Rev 66, 413–434 (2014). [PubMed: 24515647]
5. Milligan G, The role of dimerisation in the cellular trafficking of G-protein-coupled receptors. Curr Opin Pharmacol (2009).
6. Gomes I, Ayoub MA, Fujita W, Jaeger WC, Pfleger KD, Devi LA, G Protein-Coupled Receptor Heteromers. Annu Rev Pharmacol Toxicol 56, 403–425 (2016). [PubMed: 26514203]
7. Frangaj A, Fan QR, Structural biology of GABAB receptor. Neuropharmacology 136, 68–79 (2018). [PubMed: 29031577]
8. Pin JP, Bettler B, Organization and functions of mGlu and GABAB receptor complexes. Nature 540, 60–68 (2016). [PubMed: 27905440]
9. Niswender CM, Conn PJ, Metabotropic glutamate receptors: physiology, pharmacology, and disease. Annu Rev Pharmacol Toxicol 50, 295–322 (2010). [PubMed: 20055706]
10. Hebert TE, Moffett S, Morello JP, Loisel TP, Bichet DG, Barret C, Bouvier M, A peptide derived from a beta2-adrenergic receptor transmembrane domain inhibits both receptor dimerization and activation. J Biol Chem 271, 16384–16392 (1996). [PubMed: 8663163]
11. Gonzalez-Maeso J, GPCR oligomers in pharmacology and signaling. Mol Brain 4, 20 (2011). [PubMed: 21619615]
12. Gaitonde SA, Gonzalez-Maeso J, Contribution of heteromerization to G protein-coupled receptor function. Curr Opin Pharmacol 32, 23–31 (2017). [PubMed: 27835800]

13. Lan TH, Liu Q, Li C, Wu G, Steyaert J, Lambert NA, BRET evidence that beta2 adrenergic receptors do not oligomerize in cells. Sci Rep 5, 10166 (2015). [PubMed: 25955971]
14. Milligan G, Bouvier M, Methods to monitor the quaternary structure of G protein-coupled receptors. Febs J 272, 2914–2925 (2005). [PubMed: 15955052]
15. Han Y, Moreira IS, Urizar E, Weinstein H, Javitch JA, Allosteric communication between protomers of dopamine class A GPCR dimers modulates activation. Nat Chem Biol 5, 688–695 (2009). [PubMed: 19648932]
16. Whorton MR, Jastrzebska B, Park PS, Fotiadis D, Engel A, Palczewski K, Sunahara RK, Efficient coupling of transducin to monomeric rhodopsin in a phospholipid bilayer. J Biol Chem 283, 4387–4394 (2008). [PubMed: 18033822]
17. Ge B, Lao J, Li J, Chen Y, Song Y, Huang F, Single-molecule imaging reveals dimerization/oligomerization of CXCR4 on plasma membrane closely related to its function. Sci Rep 7, 16873 (2017). [PubMed: 29203889]
18. Sartania N, Appelbe S, Pediani JD, Milligan G, Agonist occupancy of a single monomeric element is sufficient to cause internalization of the dimeric beta2-adrenoceptor. Cell Signal 19, 1928–1938 (2007). [PubMed: 17561373]
19. Lopez-Gimenez JF, Canals M, Pediani JD, Milligan G, The alpha1b-adrenoceptor exists as a higher-order oligomer: effective oligomerization is required for receptor maturation, surface delivery, and function. Mol Pharmacol 71, 1015–1029 (2007). [PubMed: 17220353]
20. Smith TH, Li JG, Dores MR, Trejo J, Protease-activated receptor-4 and purinergic receptor P2Y12 dimerize, co-internalize, and activate Akt signaling via endosomal recruitment of beta-arrestin. J Biol Chem 292, 13867–13878 (2017). [PubMed: 28652403]
21. Jin J, Momboisse F, Boncompain G, Koensgen F, Zhou Z, Cordeiro N, Arenzana-Seisdedos F, Perez F, Lagane B, Kellenberger E, Brelot A, CCR5 adopts three homodimeric conformations that control cell surface delivery. Sci Signal 11, (2018).
22. Marsango S, Caltabiano G, Jimenez-Roses M, Millan MJ, Pediani JD, Ward RJ, Milligan G, A Molecular Basis for Selective Antagonist Destabilization of Dopamine D3 Receptor Quaternary Organization. Sci Rep 7, 2134 (2017). [PubMed: 28522847]
23. Dijkman PM, Castell OK, Goddard AD, Munoz-Garcia JC, de Graaf C, Wallace MI, Watts A, Dynamic tuneable G protein-coupled receptor monomer-dimer populations. Nat Commun 9, 1710 (2018). [PubMed: 29703992]
24. Dorsch S, Klotz KN, Engelhardt S, Lohse MJ, Bunemann M, Analysis of receptor oligomerization by FRAP microscopy. Nat Methods 6, 225–230 (2009). [PubMed: 19234451]
25. Pediani JD, Ward RJ, Godin AG, Marsango S, Milligan G, Dynamic Regulation of Quaternary Organization of the M1 Muscarinic Receptor by Subtype-selective Antagonist Drugs. J Biol Chem 291, 13132–13146 (2016). [PubMed: 27080256]
26. Kasai RS, Suzuki KG, Prossnitz ER, Koyama-Honda I, Nakada C, Fujiwara TK, Kusumi A, Full characterization of GPCR monomer-dimer dynamic equilibrium by single molecule imaging. J Cell Biol 192, 463–480 (2011). [PubMed: 21300851]
27. Hern JA, Baig AH, Mashanov GI, Birdsall B, Corrie JE, Lazareno S, Molloy JE, Birdsall NJ, Formation and dissociation of M1 muscarinic receptor dimers seen by total internal reflection fluorescence imaging of single molecules. Proc Natl Acad Sci U S A 107, 2693–2698 (2010). [PubMed: 20133736]
28. Meral D, Provasi D, Prada-Gracia D, Moller J, Marino K, Lohse MJ, Filizola M, Molecular details of dimerization kinetics reveal negligible populations of transient micro-opioid receptor homodimers at physiological concentrations. Sci Rep 8, 7705 (2018). [PubMed: 29769636]
29. Felce JH, Latty SL, Knox RG, Mattick SR, Lui Y, Lee SF, Klenerman D, Davis SJ, Receptor Quaternary Organization Explains G Protein-Coupled Receptor Family Structure. Cell Rep 20, 2654–2665 (2017). [PubMed: 28903045]
30. Gavalas A, Lan TH, Liu Q, Correa IR Jr., Javitch JA, Lambert NA, Segregation of family A G protein-coupled receptor protomers in the plasma membrane. Mol Pharmacol 84, 346–352 (2013). [PubMed: 23778362]
31. Dong C, Filipeanu CM, Duvernay MT, Wu G, Regulation of G protein-coupled receptor export trafficking. Biochim Biophys Acta 1768, 853–870 (2007). [PubMed: 17074298]

32. Pavlos NJ, Friedman PA, GPCR Signaling and Trafficking: The Long and Short of It. Trends Endocrinol Metab 28, 213–226 (2017). [PubMed: 27889227]
33. Magalhaes AC, Dunn H, Ferguson SS, Regulation of GPCR activity, trafficking and localization by GPCR-interacting proteins. Br J Pharmacol 165, 1717–1736 (2012). [PubMed: 21699508]
34. von Zastrow M, Williams JT, Modulating neuromodulation by receptor membrane traffic in the endocytic pathway. Neuron 76, 22–32 (2012). [PubMed: 23040804]
35. Thomsen ARB, Jensen DD, Hicks GA, Bunnett NW, Therapeutic Targeting of Endosomal G-Protein-Coupled Receptors. Trends Pharmacol Sci (2018).
36. Seachrist JL, Ferguson SS, Regulation of G protein-coupled receptor endocytosis and trafficking by Rab GTPases. Life Sci 74, 225–235 (2003). [PubMed: 14607250]
37. Canals M, Lopez-Gimenez JF, Milligan G, Cell surface delivery and structural re-organization by pharmacological chaperones of an oligomerization-defective alpha(1b)-adrenoceptor mutant demonstrates membrane targeting of GPCR oligomers. Biochem J 417, 161–172 (2009). [PubMed: 18764782]
38. Lopez-Gimenez JF, Vilaro MT, Milligan G, Morphine desensitization, internalization, and down-regulation of the mu opioid receptor is facilitated by serotonin 5-hydroxytryptamine2A receptor coactivation. Mol Pharmacol 74, 1278–1291 (2008). [PubMed: 18703670]
39. Magalhaes AC, Holmes KD, Dale LB, Comps-Agrar L, Lee D, Yadav PN, Drysdale L, Poulter MO, Roth BL, Pin J-P, Anisman H, Ferguson SSG, CRF receptor 1 regulates anxiety behavior via sensitization of 5-HT2 receptor signaling. Nature neuroscience 13, 622–629 (2010). [PubMed: 20383137]
40. Gonzalez-Maeso J, Sealfon SC, Psychedelics and schizophrenia. Trends Neurosci 32, 225–232 (2009). [PubMed: 19269047]
41. Hanks JB, Gonzalez-Maeso J, Animal models of serotonergic psychedelics. ACS Chem Neurosci 4, 33–42 (2013). [PubMed: 23336043]
42. Aghajanian GK, Marek GJ, Serotonin model of schizophrenia: emerging role of glutamate mechanisms. Brain Res Brain Res Rev 31, 302–312 (2000). [PubMed: 10719157]
43. Gonzalez-Maeso J, Ang RL, Yuen T, Chan P, Weisstaub NV, Lopez-Gimenez JF, Zhou M, Okawa Y, Callado LF, Milligan G, Gingrich JA, Filizola M, Meana JJ, Sealfon SC, Identification of a serotonin/glutamate receptor complex implicated in psychosis. Nature 452, 93–97 (2008). [PubMed: 18297054]
44. Fribourg M, Moreno JL, Holloway T, Provasi D, Baki L, Mahajan R, Park G, Adney SK, Hatcher C, Eltit JM, Ruta JD, Albizu L, Li Z, Umali A, Shim J, Fabiato A, Mackerell AD Jr., Brezina V, Sealfon SC, Filizola M, Gonzalez-Maeso J, Logothetis DE, Decoding the Signaling of a GPCR Heteromeric Complex Reveals a Unifying Mechanism of Action of Antipsychotic Drugs. Cell 147, 1011–1023 (2011). [PubMed: 22118459]
45. Moreno JL, Muguruza C, Umali A, Mortillo S, Holloway T, Pilar-Cuellar F, Mocci G, Seto J, Callado LF, Neve RL, Milligan G, Sealfon SC, Lopez-Gimenez JF, Meana JJ, Benson DL, Gonzalez-Maeso J, Identification of three residues essential for 5-hydroxytryptamine 2A-metabotropic glutamate 2 (5-HT2A.mGlu2) receptor heteromerization and its psychoactive behavioral function. J Biol Chem 287, 44301–44319 (2012). [PubMed: 23129762]
46. Baki L, Fribourg M, Younkin J, Eltit JM, Moreno JL, Park G, Vysotskaya Z, Narahari A, Sealfon SC, Gonzalez-Maeso J, Logothetis DE, Cross-signaling in metabotropic glutamate 2 and serotonin 2A receptor heteromers in mammalian cells. Pflugers Arch 468, 775–793 (2016). [PubMed: 26780666]
47. Moreno JL, Miranda-Azpiazu P, Garcia-Bea A, Younkin J, Cui M, Kozlenkov A, Ben-Ezra A, Voloudakis G, Fakira AK, Baki L, Ge Y, Georgakopoulos A, Moron JA, Milligan G, Lopez-Gimenez JF, Robakis NK, Logothetis DE, Meana JJ, Gonzalez-Maeso J, Allosteric signaling through an mGlu2 and 5-HT2A heteromeric receptor complex and its potential contribution to schizophrenia. Sci Signal 9, ra5 (2016). [PubMed: 26758213]
48. Rives ML, Vol C, Fukazawa Y, Tinel N, Trinquet E, Ayoub MA, Shigemoto R, Pin JP, Prezeau L, Crosstalk between GABAB and mGlu1a receptors reveals new insight into GPCR signal integration. EMBO J 28, 2195–2208 (2009). [PubMed: 19590495]

49. Delille HK, Becker JM, Burkhardt S, Bleher B, Terstappen GC, Schmidt M, Meyer AH, Unger L, Marek GJ, Mezler M, Heterocomplex formation of 5-HT(2A)-mGlu(2) and its relevance for cellular signaling cascades. Neuropharmacology 1–8 (2012).
50. Olivero G, Grilli M, Vergassola M, Bonfiglio T, Padolecchia C, Garrone B, Di Giorgio FP, Tongiani S, Usai C, Marchi M, Pittaluga A, 5-HT2A-mGlu2/3 receptor complex in rat spinal cord glutamatergic nerve endings: A 5-HT2A to mGlu2/3 signalling to amplify presynaptic mechanism of auto-control of glutamate exocytosis. Neuropharmacology 133, 429–439 (2018). [PubMed: 29499271]
51. Hamor PU, Sirova J, Palenicek T, Zaniewska M, Bubenikova-Valesova V, Schwendt M, Chronic methamphetamine self-administration dysregulates 5-HT2A and mGlu2 receptor expression in the rat prefrontal and perirhinal cortex: Comparison to chronic phencyclidine and MK-801. Pharmacol Biochem Behav 175, 89–100 (2018). [PubMed: 30240581]
52. Bermak JC, Li M, Bullock C, Zhou QY, Regulation of transport of the dopamine D1 receptor by a new membrane-associated ER protein. Nat Cell Biol 3, 492–498 (2001). [PubMed: 11331877]
53. Petaja-Repo UE, Hogue M, Laperriere A, Walker P, Bouvier M, Export from the endoplasmic reticulum represents the limiting step in the maturation and cell surface expression of the human delta opioid receptor. J Biol Chem 275, 13727–13736 (2000). [PubMed: 10788493]
54. Jacobsen SE, Ammendrup-Johnsen I, Jansen AM, Gether U, Madsen KL, Brauner-Osborne H, The GPRC6A receptor displays constitutive internalization and sorting to the slow recycling pathway. J Biol Chem 292, 6910–6926 (2017). [PubMed: 28280242]
55. Schmid CL, Raehal KM, Bohn LM, Agonist-directed signaling of the serotonin 2A receptor depends on beta-arrestin-2 interactions in vivo. Proc Natl Acad Sci U S A 105, 1079–1084 (2008). [PubMed: 18195357]
56. Cornea-Hebert V, Riad M, Wu C, Singh SK, Descarries L, Cellular and subcellular distribution of the serotonin 5-HT2A receptor in the central nervous system of adult rat. J Comp Neurol 409, 187–209 (1999). [PubMed: 10379914]
57. Cornea-Hebert V, Watkins KC, Roth BL, Kroeze WK, Gaudreau P, Leclerc N, Descarries L, Similar ultrastructural distribution of the 5-HT(2A) serotonin receptor and microtubule-associated protein MAP1A in cortical dendrites of adult rat. Neuroscience 113, 23–35 (2002). [PubMed: 12123681]
58. Doherty MD, Pickel VM, Ultrastructural localization of the serotonin 2A receptor in dopaminergic neurons in the ventral tegmental area. Brain Res 864, 176–185 (2000). [PubMed: 10802024]
59. Jakab RL, Goldman-Rakic PS, 5-Hydroxytryptamine2A serotonin receptors in the primate cerebral cortex: possible site of action of hallucinogenic and antipsychotic drugs in pyramidal cell apical dendrites. Proc Natl Acad Sci U S A 95, 735–740 (1998). [PubMed: 9435262]
60. Ibi D, de la Fuente Revenga M, Kezunovic N, Muguruza C, Saunders JM, Gaitonde SA, Moreno JL, Ijaz MK, Santosh V, Kozlenkov A, Holloway T, Seto J, Garcia-Bea A, Kurita M, Mosley GE, Jiang Y, Christoffel DJ, Callado LF, Russo SJ, Dracheva S, Lopez-Gimenez JF, Ge Y, Escalante CR, Meana JJ, Akbarian S, Huntley GW, Gonzalez-Maeso J, Antipsychotic-induced Hdac2 transcription via NF-kappaB leads to synaptic and cognitive side effects. Nat Neurosci 20, 1247–1259 (2017). [PubMed: 28783139]
61. Kerppola TK, Visualization of molecular interactions by fluorescence complementation. Nat Rev Mol Cell Biol 7, 449–456 (2006). [PubMed: 16625152]
62. Soto CA, Shashack MJ, Fox RG, Bubar MJ, Rice KC, Watson CS, Cunningham KA, Gilbertson SR, Anastasio NC, Novel Bivalent 5-HT2A Receptor Antagonists Exhibit High Affinity and Potency in Vitro and Efficacy in Vivo. ACS Chem Neurosci 9, 514–521 (2018). [PubMed: 29111677]
63. Iglesias A, Cimadevila M, Cadavid MI, Loza MI, Brea J, Serotonin-2A homodimers are needed for signalling via both phospholipase A2 and phospholipase C in transfected CHO cells. Eur J Pharmacol 800, 63–69 (2017). [PubMed: 28216047]
64. Herrick-Davis K, Weaver BA, Grinde E, Mazurkiewicz JE, Serotonin 5-HT2C receptor homodimer biogenesis in the endoplasmic reticulum: real-time visualization with confocal fluorescence resonance energy transfer. J Biol Chem 281, 27109–27116 (2006). [PubMed: 16857671]

65. Ward RJ, Alvarez-Curto E, Milligan G, Using the Flp-In T-Rex system to regulate GPCR expression. Methods Mol Biol 746, 21–37 (2011). [PubMed: 21607850]
66. Murat S, Bigot M, Chapron J, Konig GM, Kostenis E, Battaglia G, Nicoletti F, Bourinet E, Bockaert J, Marin P, Vandermoere F, 5-HT2A receptor-dependent phosphorylation of mGlu2 receptor at Serine 843 promotes mGlu2 receptor-operated Gi/o signaling. Mol Psychiatry (2018).
67. Poulie CBM, Liu N, Jensen AA, Bunch L, Design, Synthesis, and Pharmacological Characterization of Heterobivalent Ligands for the Putative 5-HT2A/mGlu2 Receptor Complex. J Med Chem (2020).
68. Arsenovic PT, Mayer CR, Conway DE, SensorFRET: A Standardless Approach to Measuring Pixel-based Spectral Bleed-through and FRET Efficiency using Spectral Imaging. Sci Rep 7, 15609 (2017). [PubMed: 29142199]
69. Gomes I, Sierra S, Devi LA, Detection of Receptor Heteromerization Using In Situ Proximity Ligation Assay. Curr Protoc Pharmacol 75, 2 16 11–12 16 31 (2016). [PubMed: 27960030]
70. Sorkin A, von Zastrow M, Endocytosis and signalling: intertwining molecular networks. Nat Rev Mol Cell Biol 10, 609–622 (2009). [PubMed: 19696798]
71. Basiji DA, Ortyn WE, Liang L, Venkatachalam V, Morrissey P, Cellular image analysis and imaging by flow cytometry. Clin Lab Med 27, 653–670, viii (2007). [PubMed: 17658411]
72. Wagstaff KM, Jans DA, Protein transduction: cell penetrating peptides and their therapeutic applications. Curr Med Chem 13, 1371–1387 (2006). [PubMed: 16719783]
73. Moreno JL, Muguruza C, Umali A, Mortillo S, Holloway T, Pilar-Cuellar F, Mocci G, Seto J, Callado LF, Neve RL, Milligan G, Sealfon SC, Lopez-Gimenez JF, Meana JJ, Benson DL, Gonzalez-Maeso J, Identification of three residues essential for 5-hydroxytryptamine 2A-metabotropic glutamate 2 (5-HT2A.mGlu2) receptor heteromerization and its psychoactive behavioral function. J Biol Chem 287, 44301–44319 [PubMed: 23129762]
74. Kotowski SJ, Hopf FW, Seif T, Bonci A, Von Zastrow M, Endocytosis promotes rapid dopaminergic signaling. Neuron 71, 278–290 (2011). [PubMed: 21791287]
75. Meltzer HY, Update on typical and atypical antipsychotic drugs. Annu Rev Med 64, 393–406 (2013). [PubMed: 23020880]
76. de la Fuente Revenga M, Ibi D, Cuddy T, Toneatti R, Kurita M, Ijaz MK, Miles MF, Wolstenholme JT, Gonzalez-Maeso J, Chronic clozapine treatment restrains via HDAC2 the performance of mGlu2 receptor agonism in a rodent model of antipsychotic activity. Neuropsychopharmacology (2018).
77. Kurita M, Holloway T, Garcia-Bea A, Kozlenkov A, Friedman AK, Moreno JL, Heshmati M, Golden SA, Kennedy PJ, Takahashi N, Dietz DM, Mocci G, Gabilondo AM, Hanks J, Umali A, Callado LF, Gallitano AL, Neve RL, Shen L, Buxbaum JD, Han MH, Nestler EJ, Meana JJ, Russo SJ, Gonzalez-Maeso J, HDAC2 regulates atypical antipsychotic responses through the modulation of mGlu2 promoter activity. Nat Neurosci 15, 1245–1254 (2012). [PubMed: 22864611]
78. Tashiro A, Yuste R, Structure and molecular organization of dendritic spines. Histol Histopathol 18, 617–634 (2003). [PubMed: 12647812]
79. Spruston N, Pyramidal neurons: dendritic structure and synaptic integration. Nat Rev Neurosci 9, 206–221 (2008). [PubMed: 18270515]
80. Koleske AJ, Molecular mechanisms of dendrite stability. Nat Rev Neurosci 14, 536–550 (2013). [PubMed: 23839597]
81. Lopez-Gimenez JF, Alvarez-Curto E, Milligan G, M3 muscarinic acetylcholine receptor facilitates the endocytosis of mu opioid receptor mediated by morphine independently of the formation of heteromeric complexes. Cell Signal 35, 208–222 (2017). [PubMed: 28411124]
82. Jordan BA, Trapaidze N, Gomes I, Nivarthi R, Devi LA, Oligomerization of opioid receptors with beta 2-adrenergic receptors: a role in trafficking and mitogen-activated protein kinase activation. Proc Natl Acad Sci U S A 98, 343–348 (2001). [PubMed: 11134510]
83. Xu J, He J, Castleberry AM, Balasubramanian S, Lau AG, Hall RA, Heterodimerization of alpha 2A- and beta 1-adrenergic receptors. J Biol Chem 278, 10770–10777 (2003). [PubMed: 12529373]
84. Hillion J, Canals M, Torvinen M, Casado V, Scott R, Terasmaa A, Hansson A, Watson S, Olah ME, Mallol J, Canela EI, Zoli M, Agnati LF, Ibanez CF, Lluis C, Franco R, Ferre S, Fuxe K,

Coaggregation, cointernalization, and codesensitization of adenosine A2A receptors and dopamine D2 receptors. J Biol Chem 277, 18091–18097 (2002). [PubMed: 11872740]

85. Berg KA, Maayani S, Goldfarb J, Scaramellini C, Leff P, Clarke WP, Effector pathway-dependent relative efficacy at serotonin type 2A and 2C receptors: evidence for agonist-directed trafficking of receptor stimulus. Mol Pharmacol 54, 94–104 (1998). [PubMed: 9658194]
86. Calebiro D, Rieken F, Wagner J, Sungkaworn T, Zabel U, Borzi A, Cocucci E, Zurn A, Lohse MJ, Single-molecule analysis of fluorescently labeled G-protein-coupled receptors reveals complexes with distinct dynamics and organization. Proc Natl Acad Sci U S A 110, 743–748 (2013). [PubMed: 23267088]
87. Crilly J, The history of clozapine and its emergence in the US market: a review and analysis. History of Psychiatry 18, 30–60 (2007).
88. Lieberman JA, Bymaster FP, Meltzer HY, Deutch AY, Duncan GE, Marx CE, Aprille JR, Dwyer DS, Li XM, Mahadik SP, Duman RS, Porter JH, Modica-Napolitano JS, Newton SS, Csernansky JG, Antipsychotic drugs: comparison in animal models of efficacy, neurotransmitter regulation, and neuroprotection. Pharmacol Rev 60, 358–403 (2008). [PubMed: 18922967]
89. Miyamoto S, Miyake N, Jarskog LF, Fleischhacker WW, Lieberman JA, Pharmacological treatment of schizophrenia: a critical review of the pharmacology and clinical effects of current and future therapeutic agents. Mol Psychiatry 17, 1206–1227 (2012). [PubMed: 22584864]
90. Patil ST, Zhang L, Martenyi F, Lowe SL, Jackson KA, Andreev BV, Avedisova AS, Bardenstein LM, Gurovich IY, Morozova MA, Mosolov SN, Neznanov NG, Reznik AM, Smulevich AB, Tochilov VA, Johnson BG, Monn JA, Schoepp DD, Activation of mGlu2/3 receptors as a new approach to treat schizophrenia: a randomized Phase 2 clinical trial. Nat Med 13, 1102–1107 (2007). [PubMed: 17767166]
91. Ellaithy A, Younkin J, Gonzalez-Maeso J, Logothetis DE, Positive allosteric modulators of metabotropic glutamate 2 receptors in schizophrenia treatment. Trends Neurosci 38, 506–516 (2015). [PubMed: 26148747]
92. Kinon BJ, Millen BA, Zhang L, McKinzie DL, Exploratory Analysis for a Targeted Patient Population Responsive to the Metabotropic Glutamate 2/3 Receptor Agonist Pomaglumetad Methionil in Schizophrenia. Biol Psychiatry (2015).
93. Xue L, Rovira X, Scholler P, Zhao H, Liu J, Pin JP, Rondard P, Major ligand-induced rearrangement of the heptahelical domain interface in a GPCR dimer. Nat Chem Biol 11, 134–140 (2015). [PubMed: 25503927]
94. Gonzalez-Maeso J, Weisstaub NV, Zhou M, Chan P, Ivic L, Ang R, Lira A, Bradley-Moore M, Ge Y, Zhou Q, Sealfon SC, Gingrich JA, Hallucinogens Recruit Specific Cortical 5-HT(2A) Receptor-Mediated Signaling Pathways to Affect Behavior. Neuron 53, 439–452 (2007). [PubMed: 17270739]
95. Bajar BT, Wang ES, Zhang S, Lin MZ, Chu J, A Guide to Fluorescent Protein FRET Pairs. Sensors (Basel) 16, (2016).
96. Chaudhry FA, Lehre KP, van Lookeren Campagne M, Ottersen OP, Danbolt NC, Storm-Mathisen J, Glutamate transporters in glial plasma membranes: highly differentiated localizations revealed by quantitative ultrastructural immunocytochemistry. Neuron 15, 711–720 (1995). [PubMed: 7546749]
97. Hjelle OP, Chaudhry FA, Ottersen OP, Antisera to glutathione: characterization and immunocytochemical application to the rat cerebellum. Eur J Neurosci 6, 793–804 (1994). [PubMed: 8075821]
98. van Lookeren Campagne M, Oestreicher AB, van der Krift TP, Gispen WH, Verkleij AJ, Freeze-substitution and Lowicryl HM20 embedding of fixed rat brain: suitability for immunogold ultrastructural localization of neural antigens. J Histochem Cytochem 39, 1267–1279 (1991). [PubMed: 1833448]
99. Peters A, Palay SL, Webster H. deF., Fine Structure of the Nervous System: Neurons and Their Supporting Cells. (Oxford University Press, 1991).
100. Dunn KW, Kamocka MM, McDonald JH, A practical guide to evaluating colocalization in biological microscopy. Am J Physiol Cell Physiol 300, C723–742 (2011). [PubMed: 21209361]

101. Adler J, Parmryd I, Quantifying colocalization by correlation: the Pearson correlation coefficient is superior to the Mander's overlap coefficient. Cytometry A 77, 733–742 (2010). [PubMed: 20653013]

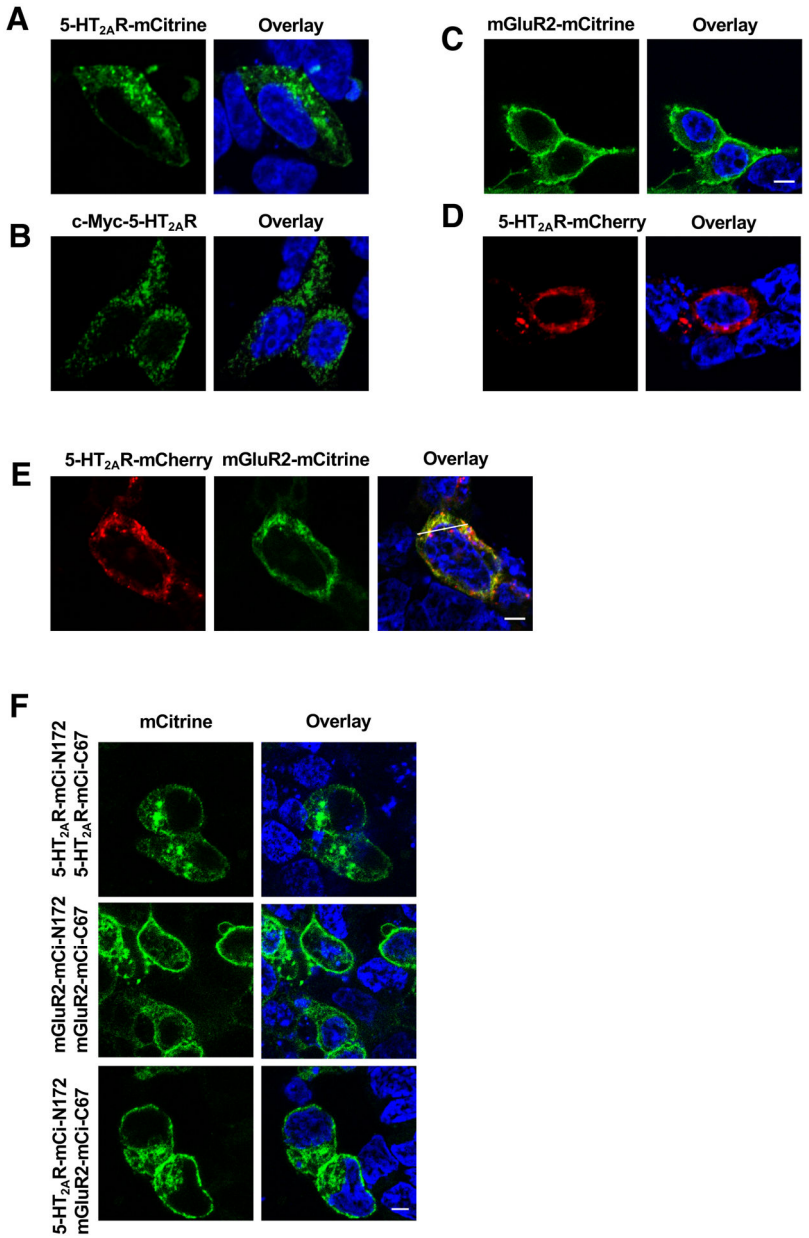

Fig. 1. 5-HT$_{2A}$R affects localization of mGluR2.

(**A** and **B**) Representative confocal micrographs of HEK293 cells transfected to express 5-HT$_{2A}$R-mCitrine (**A**) or c-Myc-5-HT$_{2A}$R (**B**). Nonpermeabilized cells were imaged to detect mCitrine (**A**), whereas permeabilized cells were stained with anti-c-Myc and secondary antibody, and imaged to detect anti-c-Myc (**B**). (**C** to **E**) HEK293 cells were transfected to express mGluR2-mCitrine alone (**C**), 5-HT$_{2A}$R-mCherry alone (**D**), or 5-HT$_{2A}$R-mCherry and mGluR2-mCitrine (**E**; for the corresponding line scan, see fig. S1A). (**F**) BiFC signal in HEK293 cells transfected to coexpress 5-HT$_{2A}$R-mCi-N172 and 5-HT$_{2A}$R-mCi-C67, 5-HT$_{2A}$R-mCi-N172 and mGluR2-mCi-C67, or 5-HT$_{2A}$R-mCi-N172 and mGluR2-mCi-C67. Nuclei were stained in blue with Hoechst. Scale bars, 5 μm.

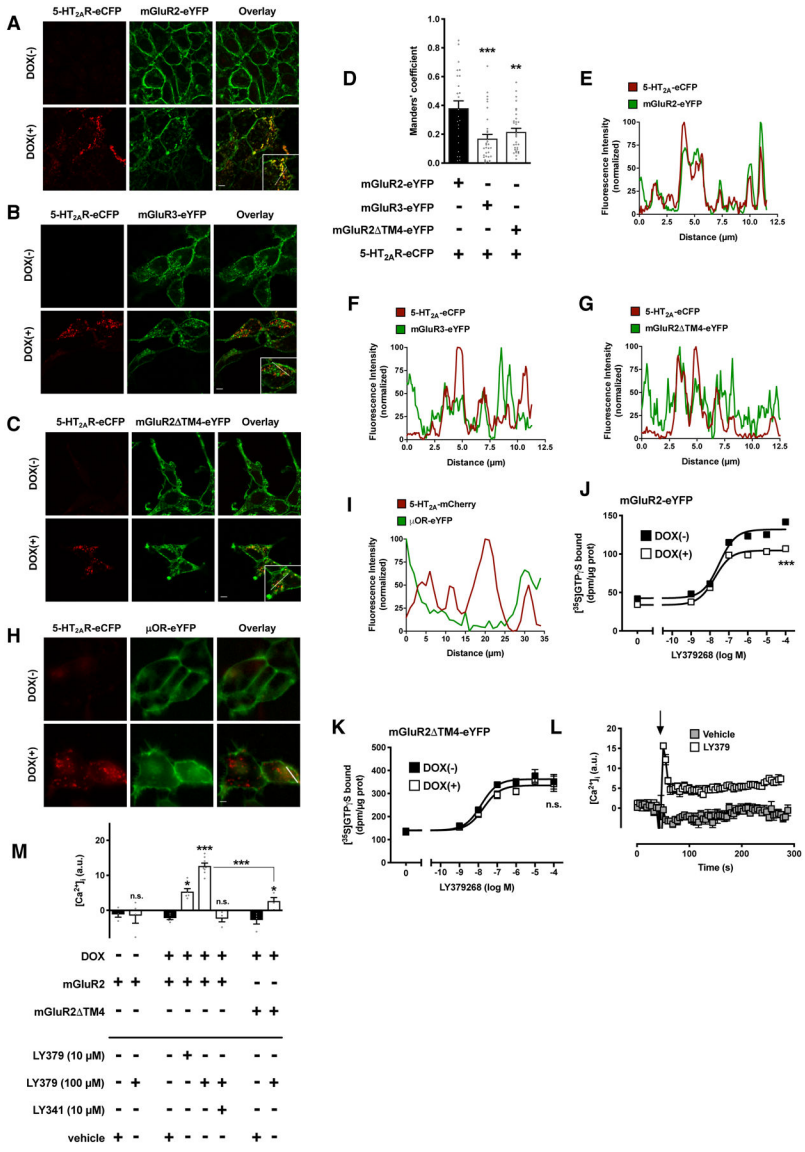

Fig. 2. Effect of 5-HT$_{2A}$R on localization of mGluR2 requires heteromerization.

(**A** to **I**) Flp-In T-REx HEK293 cells stably expressing mGluR2-eYFP (**A**, **D** and **E**), mGluR3-eYFP (**B**, **D** and **F**), mGluR2ΔTM4-eYFP (**C**, **D** and **G**), or μOR-eYFP (**H** and **I**) and harboring 5-HT$_{2A}$R-eCFP at the inducible locus were left untreated [DOX(−)] or treated with doxycycline [DOX(+)]. Representative confocal micrographs (**A** to **C** and **H**) and corresponding line scans (**E** to **I**). (**D**) Manders' coefficient colocalization analysis of eYFP- and eCFP-tagged constructs (n = 25 – 33 cell regions of interest in three independent experiments). (**J** a vvnd **K**) Effect of the mGluR2/3 agonist LY379268 on [^{35}S]GTPγS binding in membrane preparations of Flp-In T-REx HEK293 cells stably expressing mGluR2-eYFP (**J**) or mGluR2ΔTM4-eYFP (**K**) and harboring 5-HT$_{2A}$R-eCFP at the inducible locus. Cells were left untreated [DOX(−)] or treated with doxycycline [DOX(+)] (representative results of three independent experiments performed in duplicate). (**L** and **M**) Flp-In T-REx HEK293 cells stably expressing mGluR2-eYFP or mGluR2ΔTM4-eYFP and harboring 5-HT$_{2A}$R-eCFP at the inducible locus were left untreated [DOX(−)] or treated

with doxycycline [DOX(+)], loaded with Fura-2 and monitored for intracellular Ca^{2+} concentration ($[Ca^{2+}]_i$) after sequential administration of LY341495 and/or LY379268, or vehicle. Representative time course of Ca^{2+} release. The arrowhead indicates the time when drugs were added (**L**). Analysis of the fold increase in intracellular calcium concentration (**M**; n = 4 – 8 independent experiments). Data are mean ± SEM (**D** and **J** to **M**). Statistical analysis was performed using the one-way (**D**) or two-way (**M**) ANOVA with Bonferroni's post hoc test, or the *F* test (**J** and **K**). *$P < 0.05$, **$P < 0.01$, ***$P < 0.001$, n.s., not significant. Scale bars, 5 μm.

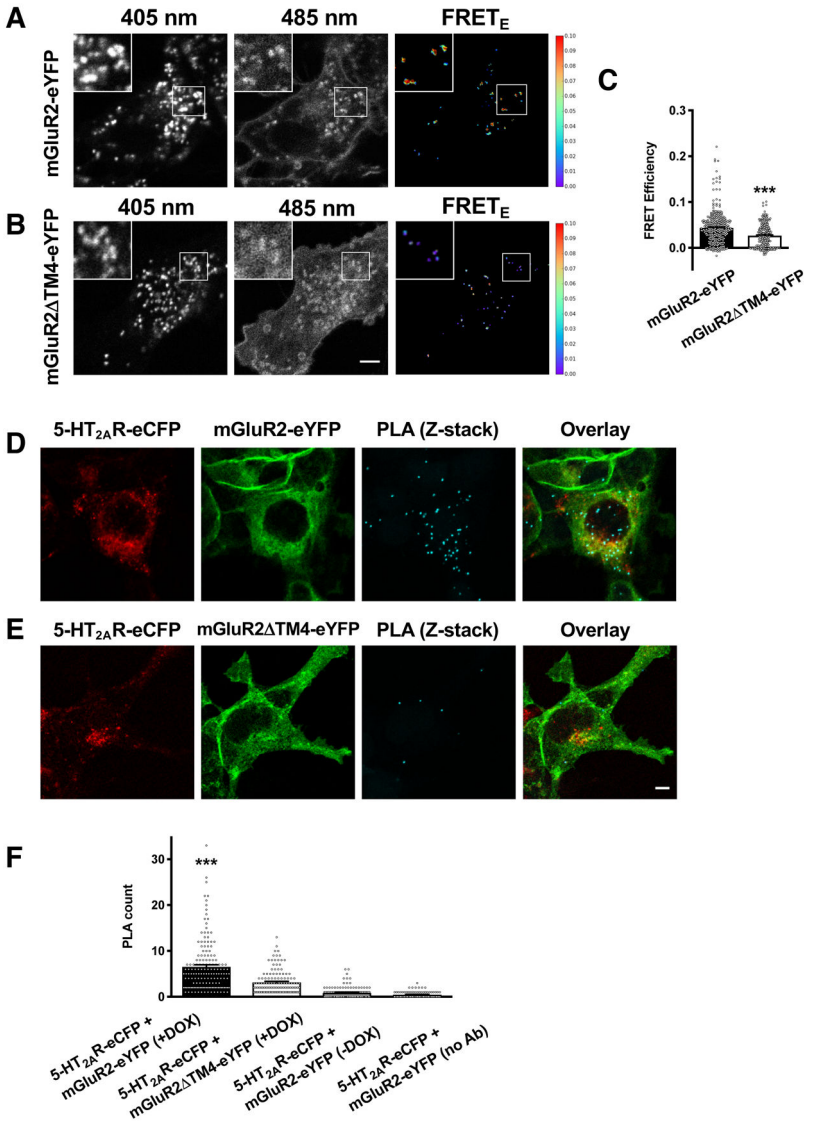

Fig. 3. Intracellular localization of the 5-HT$_{2A}$R-mGluR2 complex.

(**A** to **C**) SensorFRET analysis of Flp-In T-REx HEK293 cells stably expressing mGluR2-eYFP (**A** and **C**) or mGluR2ΔTM4-eYFP (**B** and **C**), harboring 5-HT$_{2A}$R-eCFP at the inducible locus, and treated with doxycycline. Representative live-cell confocal images at 405 nm and 458 nm excitation frequencies (**A** and **B**), and quantification (**C**) of FRET efficiencies (n = 249 – 364 regions of interest in three independent experiments). (**D** to **F**) Flp-In T-REx HEK293 cells stably expressing mGluR2-eYFP (**D** and **F**) or mGluR2ΔTM4-eYFP (**E** and **F**) and harboring c-Myc-5-HT$_{2A}$R-eCFP at the inducible locus were treated with doxycycline, permeabilized and stained with anti-rabbit antibody selective for c-Myc and anti-mouse antibody selective for mGluR2, followed by incubation with species-specific PLA probes. Representative confocal micrographs of eCFP- or eYFP-tagged constructs and PLA signal (cyan dots, Z-stack projection) (**D** and **E**). Quantification of PLA dots (**F**). Note that PLA signal was decreased in DOX(−) cells, or when primary antibodies were not added (n = 57 – 94 cell regions of interest demarcated according to eYFP signal within previously

defined eCFP-positive cells in three independent experiments). Data are median with 95% confidence interval (**C**) or mean ± SEM (**F**). Statistical analysis was performed using Mann-Whitney U test (**C**) or one-way ANOVA with Bonferroni's post hoc test (**F**). ***$P < 0.001$. Scale bars, 5 μm.

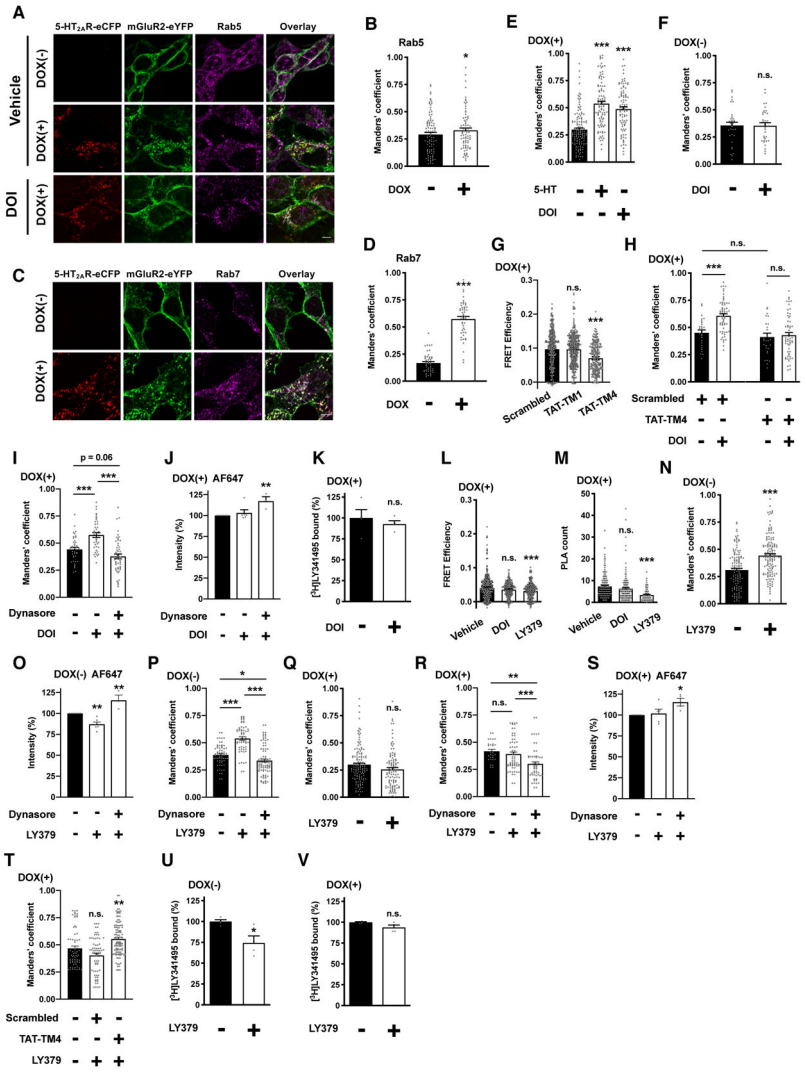

Fig. 4. Agonist activation of either 5-HT$_{2A}$R or mGluR2 differentially affects mGluR2 trafficking and downregulation.

(**A** to **F**, **N** and **Q**) Flp-In T-REx HEK293 cells stably expressing mGluR2-eYFP and harboring c-Myc-5-HT$_{2A}$R-eCFP at the inducible locus were left untreated [DOX(−)] or treated with doxycycline [DOX(+)], and exposed for 60 min to serotonin (5-HT, 1 μM), DOI (1 μM) or LY379268 (10 μM), or vehicle. Cells were then permeabilized and stained with anti-Rab5 or anti-Rab7 and secondary antibody, and imaged by confocal microscopy to detect eCFP, eYFP, anti-Rab5, or anti-Rab7. Representative confocal micrographs (**A** and **C**; for the corresponding line scan, see figs. S1B to S1F), and Manders' coefficient colocalization analysis of anti-Rab5 (**B**, **E**, **F**, **N** and **Q**; n = 33 – 134 cell regions of interest in three independent experiments) or anti-Rab7 (**D**; n = 48 – 49 cell regions of interest in three independent experiments) and eYFP-tagged construct. (**G**) Cells were incubated (60 min; 10 μM) with TAT-fused peptides corresponding to TM1 (TAT-TM1) or TM4 (TAT-TM4) of mGluR2, or scrambled control peptide and then processed for sensorFRET (n = 248 – 393 regions of interest in three independent experiments). (**H** and **T**) Manders' coefficient colocalization analysis of anti-Rab5 and eYFP-tagged construct. Cells were

exposed for 60 min to DOI (1 μM, **H**), LY379268 (10 μM, **T**), or vehicle. TAT-tagged peptides (10 μM) were added 5 min before drug or vehicle administration (n = 27 – 103 cell regions of interest in three independent experiments). (**I**, **P** and **R**) Manders' coefficient colocalization analysis of anti-Rab5 and eYFP-tagged construct. Cells were exposed for 60 min to DOI (1 μM, **I**), LY379268 (10 μM, **P** and **R**), or vehicle. Dynasore (80 μM) was added 5 min before drug or vehicle administration (n = 28 – 88 cell regions of interest in three independent experiments). (**J**, **O** and **S**) Cell surface localization of mGluR2-eYFP assessed by flow cytometry assays with an Alexa Fluor 647 (AF647)-tagged antibody. Cells were exposed for 60 min to DOI (1 μM, **J**), LY379268 (10 μM, **O** and **S**), or vehicle. Dynasore (80 μM) was added 5 min before drug or vehicle administration (n = 3 – 6 independent experiments with 8508 – 10048 cells per experimental condition). (**K**, **U** and **V**) Density of mGluR2 shown as [^{3}H]LY341495 binding in membrane preparations of DOX(+) (**K** and **V**) or DOX(−) (**U**) cells exposed for 60 min to DOI (1 μM, **K**), LY379268 (10 μM, **U** and **V**), or vehicle. Data are shown as percentage of specific binding in DOI- or LY379268-treated cells as compared to vehicle (n = 4 independent groups of membrane preparations). (**L** and **M**) Cells were exposed for 60 min to DOI (1 μM), LY379268 (10 μM), or vehicle. Quantification of FRET efficiencies (**L**, n = 281 – 536 regions of interest in three independent experiments). Quantification of PLA dots (**M**, n = 82 – 148 cell regions of interest demarcated according to eYFP signal within previously defined eCFP-positive cells in three independent experiments). Data are mean ± SEM (**B**, **D** to **F**, **H** to **K**, **M** to **V**) or median with 95% confidence interval (**G** and **L**). Statistical analysis was performed using Student's *t*-test (**B**, **D**, **F**, **K**, **N**, **Q**, **U**, **V**), one-way ANOVA with Bonferroni's post hoc test (**E**, **I**, **J**, **M**, **O**, **P**, and **R** to **T**), two-way ANOVA with Bonferroni's post hoc test (**H**), or one-way non-parametric ANOVA (Kruskal-Wallis) with Dunn's post hoc test (**G**, **L**). *$P <$ 0.05, **$P <$ 0.01, ***$P <$ 0.001, n.s., not significant. Scale bars, 5 μm.

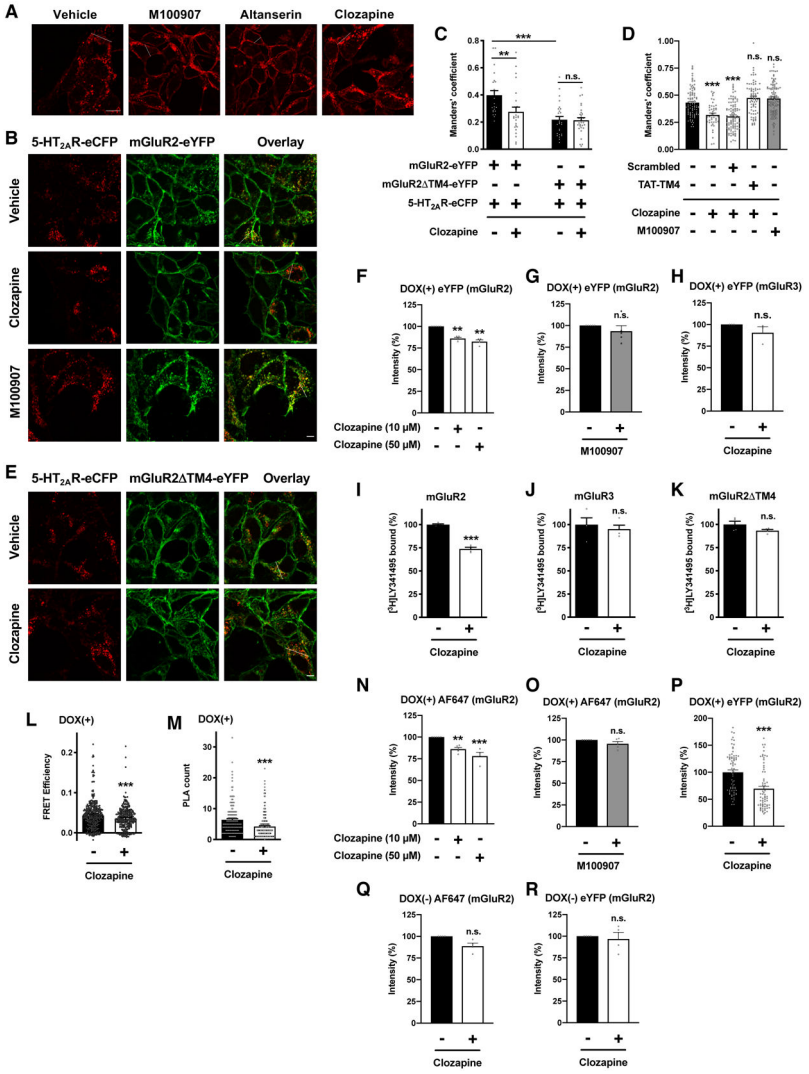

Fig. 5. Clozapine treatment affects mGluR2 trafficking and downregulation through 5-HT$_{2A}$R-mGluR2.

(**A**) Representative confocal micrographs of Flp-In T-REx HEK293 cells harboring 5-HT$_{2A}$R-eCFP at the inducible locus were treated with doxycycline, and then exposed overnight to M100907 (10 μM), altanserin (10 μM) or clozapine (10 μM), or vehicle. (**B** to **R**) Flp-In T-REx HEK293 cells stably expressing mGluR2-eYFP (**B**, **C**, **D**, **F, G**, **I**, and **L** to **R**), mGluR2ΔTM4-eYFP (**C**, **E**), or mGluR3-eYFP (**H**, **J**) and harboring 5-HT$_{2A}$R-eCFP at the inducible locus were treated with doxycycline and then exposed overnight to clozapine (10 μM or 50 μM) or M100907 (10 μM), or vehicle. Representative confocal micrographs (**A, B, E**; for the corresponding line scan, see figs. S1K to S1O). (**C**) Manders' coefficient colocalization analysis of eYFP- and eCFP-tagged constructs (n = 30 – 74 cell regions of interest in three independent experiments). (**D**) Manders' coefficient colocalization analysis of eYFP- and eCFP-tagged constructs in cells stably expressing mGluR2-eYFP and harboring 5-HT$_{2A}$R-eCFP at the inducible locus. Cells were treated with doxycycline, and then exposed overnight to clozapine (10 μM) or M100907 (10 μM), or vehicle. TAT-tagged peptides were added both 5 minutes before clozapine or vehicle administration and 65

minutes before cell fixation (n = 44 – 98 cell regions of interest in three independent experiments). (**F** to **H**, **N**, **O**, **Q**, **R**) Cell surface localization of mGluR2-eYFP with an Alexa Fluor 647 (AF647)-tagged antibody (**N**, **O**, **Q**) and mGluR2-eYFP (**F**, **G**, **R**) or mGluR3-eYFP (**H**) density with eYFP were assessed by flow cytometry assays (n = 3 – 5 independent experiments with 8148 – 10418 cells per experimental condition). (**I** to **K**) Density of mGluR2 (**I**), mGluR3 (**J**) or mGluR2ΔTM4 (**K**) shown as [^{3}H]LY341495 binding in membrane preparations of cells exposed overnight to clozapine (10 μM), or vehicle (n = 4 independent groups of membrane preparations). (**L**) Quantification of FRET efficiencies (n = 315 – 364 regions of interest in three independent experiments). (**M**) Quantification of PLA dots (n = 160 – 253 cell regions of interest demarcated according to eYFP signal within previously defined eCFP-positive cells in three independent experiments). (**P**) Intracellular eYFP signal in cells stably expressing mGluR2-eYFP and harboring 5-HT$_{2A}$R-eCFP at the inducible locus. Cells were treated with doxycycline, and then exposed overnight to clozapine (10 μM), or vehicle (n = 73 – 68 cell regions of interest demarcated based on eCFP signal within intracellular vesicles in three independent experiments). Data are mean ± SEM (**C, D, F** to **K**, and **M** to **R**) or median with 95% confidence interval (**L**). Statistical analysis was performed using Student's *t*-test (**G** to **K**, **M**, and **O** to **R**), one-way ANOVA with Bonferroni's post hoc test (**D**, **F** and **N**), two-way ANOVA with Bonferroni's post hoc test (**C**), or Mann-Whitney U test (**L**). $^{**}P < 0.01$, $^{***}P < 0.001$, n.s., not significant. Scale bars, 5 μm.

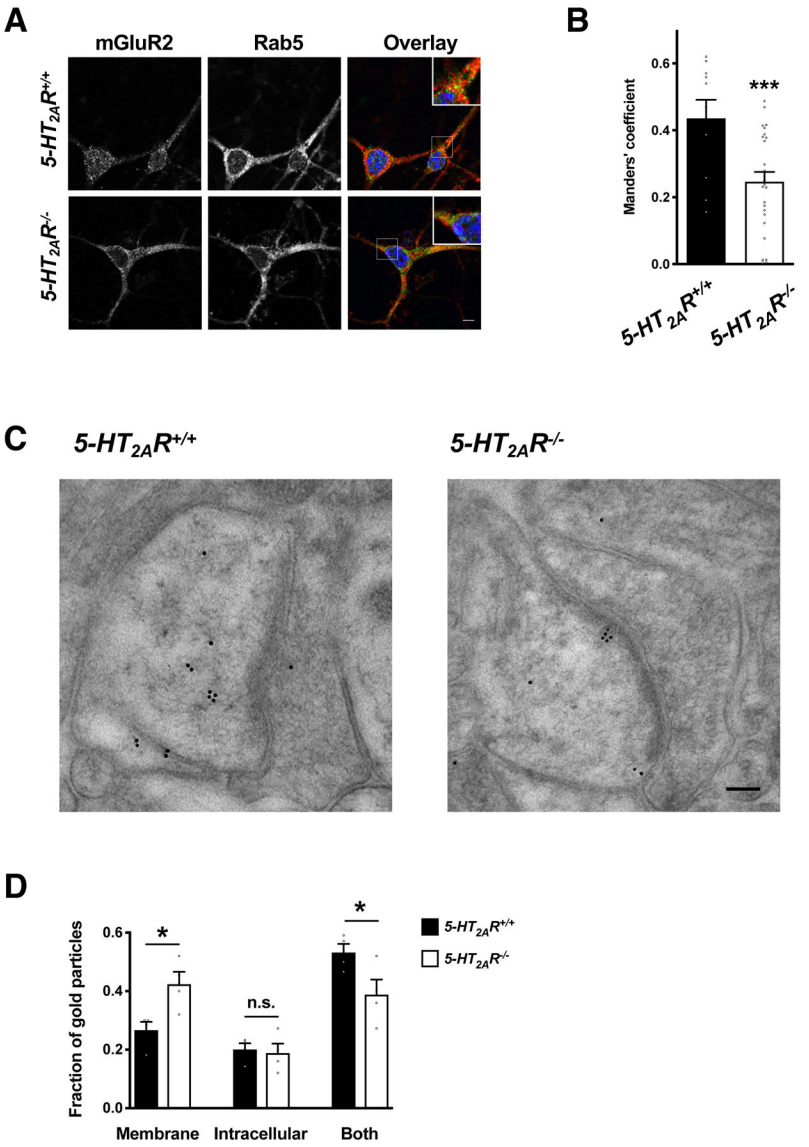

Fig. 6. Localization of mGluR2 is dysregulated in the frontal cortex of *5-HT$_{2A}$R$^{-/-}$* mice.

(A and **B)** Colocalization analysis of anti-mGluR2 and anti-Rab5 immunoreactivity in cortical primary cultures of *5-HT$_{2A}$R$^{+/+}$* and *5-HT$_{2A}$R$^{-/-}$* mice. Representative confocal micrographs (**A**). Manders' coefficient colocalization analysis (**B**; n = 30 – 74 cell regions of interest in two independent experiments). Nuclei were stained in blue with Hoechst. (**C** and **D**) Immunogold labeling for anti-mGluR2 immunoreactivity in the frontal cortex of *5-HT$_{2A}$R$^{+/+}$* and *5-HT$_{2A}$R$^{-/-}$* mice (n = 4 mice per genotype and 25 – 35 synapses per mouse). Representative photomicrographs showing excitatory synapses in mouse frontal cortex (**C**). Quantification of relative distribution of gold particles within postsynaptic spines (**C**). Data are mean ± SEM (**B** and **D**). Statistical analysis was performed using Student's *t*-test (**B**), or two-way ANOVA with Bonferroni's post hoc test (**D**). **P* < 0.05, ****P* < 0.001, n.s., not significant. Scale bars, 5 μm (**A**) and 100 nm (**C**).